Experimental study of the temperature effect on two-phase flow properties in highly permeable porous media: Application to the remediation of dense non-aqueous phase liquids (DNAPLs) in polluted soil

Nicolas Philippe, Hossein Davarzani, Stéfan Colombano, Malorie Dierick, Pierre-Yves Klein, Manuel Marcoux

Experimental study of the temperature effect on two-phase flow properties in highly permeable porous media: Application to the remediation of dense non-aqueous phase liquids (DNAPLs) in polluted soil

Nicolas Philippe[a,c], Hossein Davarzani[a], Stéfan Colombano[a], Malorie Dierick[c], Pierre-Yves Klein[c], Manuel Marcoux[b]

[a]*BRGM (French Geological Survey), 3 avenue Claude Guillemin, 45100 Orléans, France*
[b]*Institut de Mécanique des Fluides de Toulouse (IMFT), Université de Toulouse, CNRS, 31400 Toulouse, France*
[c]*REMEA, 22-24 rue Lavoisier, 92000 Nanterre, France*

Abstract

The remediation of aquifers contaminated by viscous dense non-aqueous phase liquids (DNAPLs) is a challenging problem. Coal tars are the most abundant persistent DNAPLs due to their high viscosity and complexity. Pumping processes leave considerable volume fractions of DNAPLs in the soil and demand high operational costs to reach cleaning objectives. Thermally enhanced recovery focuses on decreasing DNAPL viscosity to reduce residual saturation. The oil industry has previously applied this technique with great success for enhanced oil recovery applications. However, in soil remediation, high porous media permeabilities and product densities may invalidate those techniques. Additionally, the impacts of temperature on coal tar's physical properties have not been thoroughly discussed in available literature. Here, we investigated how coal tar's physical properties, the capillary pressure-saturation curve and the relative permeability of two-phase flow in porous media depend on the temperature and flow rate experimentally. Drainage and imbibition experiments under quasi-static (steady-state) and dynamic (unsteady-state) conditions have been carried out at 293.15 K and 323.15 K in a 1D small cell filled with 1 mm homogeneous glass beads. Two different pairs of immiscible fluids have been investigated, coal tar-water and canola oil-ethanol. Results demonstrated similar trends for temperature effect and values of fluid properties for both liquid pairs, which backs up the use of canola oil-ethanol to model coal tar-water flow. It was found that there is no temperature effect on drainage-imbibition curves or residual saturation under quasi-static conditions. In dynamic conditions, the DNAPL residual saturation decreased by 16 % when the temperature changed from 293.15 K to 323.15 K. This drop was mainly linked to decreasing viscous fingering, as well as the appearance of wetting phase films around the glass beads. Both phenomena have been observed only in dynamic experiments. A high enough pumping flow rate is needed to generate dynamic effects in the porous medium. Ethanol and oil's relative permeabilities also increase with temperature under dynamic measurement conditions. Our findings indicate that flow rate is an important parameter to consider in thermal enhanced recovery processes. These effects are not taken into account in the classically used generalized Darcy's law for modeling two-phase flow in porous media with temperature variation.

Keywords

Dense non-aqueous phase liquid, two-phase flow, capillary pressure-saturation relationship, relative permeability, thermally enhanced DNAPL recovery

Nomenclature

Symbol	Definition
Bo	Bond number (-)
Ca	Capillary number (-)
g	Gravitational acceleration (m.s^{-2})
K	Intrinsic permeability (m^{2})
k_r	Relative permeability (-)
h_c	Capillary height (m)
L	Characteristic length (m)
M	Viscosity ratio (-)
n	Van Genuchten parameter (-)
p	Pressure (Pa)
p_c	Capillary pressure (Pa)
R_0	Drop mean radius (m)
S	Saturation (-)
S_{ir}	Irreducible saturation (-)
S_r	Residual saturation (-)
T	Temperature (K)
u	Darcy velocity (m.s^{-1})
V_c	Characteristic velocity (m.s^{-1})
α	Van Genuchten parameter (m^{-1})
β	Shape factor (-)
γ	Interfacial tension (N.m^{-1})
μ	Dynamic viscosity (Pa.s)
ρ	Density (kg.m^{-3})
τ	Dynamic capillarity coefficient (Pa.s)

Subscripts

Symbol	Definition
CT	Coal tar
dis	Displaced phase
E	Ethanol
inv	Invading phase
O	Canola oil
w	Wetting phase (ethanol or water)
W	Water
nw	Non-wetting phase (canola oil or coal tar)

1. Introduction

Dense non-aqueous phase liquids (DNAPLs) are liquids denser than water and slightly soluble in water. Due to their high density, DNAPLs can deeply sink into the subsurface until reaching a less permeable layer and form a non-aqueous reservoir. Subsurface zones contaminated by DNAPLs are generally hard to delimit due to soil heterogeneity, soil dispersion, and the substantial depth of the contamination combined with gravity-driven finger flow. Thus remediating these pollutants in the aquifer is a complicated matter. DNAPL source zones are even more problematic because they may keep on dissolving toxic compounds into the groundwater. Ultimately, future health and environmental problems can arise, such as drinking water contamination or soil quality degradation.

Commonly reported DNAPL contaminants include chlorinated solvents – namely, trichloroethylene (TCE) and tetrachloroethylene (PCE) – that were previously widely used as solvents for organic materials (Schwille and Pankow, 1988). Coal tars are also a notable DNAPL found in the subsurface and are also more viscous than water. (Brown et al., 2006) have measured coal tar's dynamic viscosity on multiple sites and have found that the coal tar/water viscosity ratio can vary between 10 and 10^6 (Brown et al., 2006). This range is linked to the chemical heterogeneity in coal tar. Diagnosis and risk assessment are hard because the exact composition of coal tar is generally not identifiable. Hence, a site polluted by coal tar is difficult to clean up and the choice for an applicable recovery method has to be made on a case-by-case basis.

In our study, the focus is on coal tar source zones with high pollutant concentrations. Pumping in the subsurface through production wells is a primary step used in remediation operations. However, the pumping rate is very low for DNAPLs and the remediation could take tens to hundreds of years, which is economically unsatisfying (USEPA, 1996; Russell and Rabideau, 2000; Kavanaugh and Kresic, 2008; Navy, 2008; Newell et al., 2011). The most efficient current methods for remediating DNAPL source zones are thermal treatments (Ding et al., 2019). Generally, temperature is increased to vaporize (McDade et al., 2005; Baker et al., 2006; Baston et al., 2010) or even burn (Rein, 2009; Switzer et al., 2009; Hasan et al., 2015; Scholes et al., 2015) the pollutant. The vapors generated are then collected and treated with carbon activated filters. However, generating high-temperature fields can be dangerous for the nutritional and biological functions of the soil. (Pape et al., 2015) have shown that even if a contaminant can be completely treated at 773.15 K, the soil is unusable for future construction or industrial operations (O'Carroll et al., 2005; Pape et al., 2015). As a result, NAPL residual saturation is lower in the soil after a thermally enhanced process. Afterwards, the high soil temperature can increase the degradation rate of chemical treatments (oxidation, surfactant flooding) and biological methods (bio or phytoremediation) (Melin et al., 1998).

Hot-water flooding is another technique that has shown success in treating viscous NAPLs – light or dense – contamination. The idea is to reduce the dynamic viscosity of the NAPL by increasing its temperature. During pumping, the hot water will progressively replace the NAPL and leave residual NAPL saturation in the soil. Previous authors have shown that injecting hot water increases total NAPL recovery volumes by pumping processes (Fulton, 1991; Davis, 1997; O'Carroll and Sleep, 2007). Pumping a DNAPL phase from the subsurface can be represented by an imbibition process in porous media. The DNAPL phase is progressively pushed away from the soil and the water slowly fills the pores left vacant. Thus, it is important to analyze and better understand fluid displacements before drawing any conclusions.

To characterize the behavior of the physical system composed of DNAPL, water, and a solid matrix is still an ongoing challenge in fluid mechanics. Currently, modelling is based on the theory of

immiscible multiphase flow in porous media. In our case, DNAPL and water are represented as two separate phases, and the soil is an immobile solid matrix in which both liquids may flow. For this type of engineering application, the simultaneous flow of DNAPL and water in a porous medium is commonly described using the generalization of Darcy's law to multiphase flow for each phase (Muskat and Meres, 1936).

$$\boldsymbol{u}_i = -\frac{Kk_{r,i}(S_i)}{\mu_i}\boldsymbol{\nabla}(p_i - \rho_i \boldsymbol{g}) \quad (1)$$

where $\boldsymbol{u}_i$ is the Darcy velocity (m.s^{-1}), $\boldsymbol{g}$ the gravitational acceleration, K the permeability tensor (m^2), p_i the pressure (Pa), μ_i and ρ_i respectively the dynamic viscosity (Pa.s) and density (kg.m^{-3}). The subscript i designates the water or DNAPL phase. The main difference between Darcy's law and its extension to multiphase flow is the addition of relative permeability terms $k_{r,i}$. It signifies that each phase flows independently through a virtual porous medium of permeability $Kk_{r,i}(S_i)$. The DNAPL occupies a part of the total pore space, depending on its saturation, which reduces the volume of water that can flow through and vice versa. This equation generally holds true when there is no momentum transfer at the interface of both fluid phases (Whitaker, 1986).

The presence of the two fluid phases results in an interface that is subjected to interfacial tension at the pore scale. This interface also causes a pressure discontinuity at the macroscale, with respect to capillary pressure p_c. This is subsequently defined as the difference between the pressure of the non-wetting fluid p_{nw} and the pressure of the wetting fluid p_w.

$$p_{nw} - p_w = p_c(S_w) \quad (2)$$

Immiscible DNAPLs flowing in the aquifer can be assimilated to a two-phase flow in porous media. The dimensionless numbers controlling the actual flow pattern are respectively Bond number (Bo), capillary number (Ca), and viscosity ratio (M). In the case of the imbibition of a wetting phase inside a porous medium saturated with a non-wetting phase, these numbers can be written as:

$$Bo = \frac{(\rho_{nw} - \rho_w)gL^2}{\gamma} \quad (3)$$

$$Ca = \frac{V_c \mu_{inv}}{\gamma} \quad (4)$$

$$M = \frac{\mu_{inv}}{\mu_{dis}} \quad (5)$$

L is a characteristic length. In unconsolidated media like glass beads, L is often chosen equal to the mean particle diameter. γ is the interfacial tension between both liquid phases. V_c is a characteristic velocity representing the order of magnitude of the flow rate inside the pores. The subscripts *inv* and *dis* respectively represent the invading and displaced phase. In this work, the DNAPL and water are the invading phases during drainage and imbibition, respectively. Alternatively, the viscosity ratio may be replaced by the mobility ratio (the ratio between relative permeability and viscosity). The latter includes relative permeabilities in its calculation and can be more suitable for real porous media (Hagoort, 1974). It is possible to identify flow regimes depending on the order of magnitude of

each number. The different types of two-phase flow that occur in micro-models are classified as capillary fingering, viscous fingering, and stable displacement (Lenormand et al., 1988). According to the authors, the type of flow that promotes maximum coal tar recovery and minimizes residual DNAPL saturation is stable displacement, which occurs only for $M << 1$ and $Ca > 10^{-4}$. In practice, coal tar is much more viscous than water, and $M > 1$ in the case of pumping coal tar. The main objective of thermally enhanced oil recovery is therefore to reduce this viscosity ratio in order to decrease the mobility ratio and to promote stable displacement in the porous medium. The effect of temperature on Bond and capillary number should also be estimated in order to link those to the benefits of thermal enhancement.

McLaren et al. (2009) found that, for a soil consisting of London clays, an increase from 12°C to 30°C not only reduces the kinematic viscosity of a coal tar from 10^{-4} $m^2.s^{-1}$ to 10^{-5} $m^2.s^{-1}$, but also significantly reduces the residual saturation, despite a small variation in the capillary effect (McLaren et al., 2009). Davis, (1994), experimentally obtained a decrease in residual DNAPL saturation by heating from 10°C to 30°C without any temperature effect on interfacial tension (Davis, 1994). Sleep and Ma (1997) found only a 10% change in the interfacial tension of the PCE-water pair when heated from 20°C to 90°C (Sleep and Ma, 1997). Bachmann et al. (2002) suggest that the decrease in residual saturation is also related to a decrease in the contact angle. It can decrease by 0.03 °/°C for sand, and up to 0.26 °/°C for silts (Bachmann et al., 2002). More recently, Colombano et al. (2020) studied the thermally enhanced recovery of heavy chlorinated solvents in a highly permeable porous medium and observed no effect of temperature on residual saturation on quasi-static drainage and imbibition conditions (Colombano et al., 2020).

A few similar studies have been proposed in the past for viscous oil recovery. Koci et al. (1989) studied the effect of temperature on oil-water in unconsolidated porous media (sand) between 298.15 K and 443.15 K. The main findings were that raising temperature increased the irreducible water saturation, but also decreased the residual oil saturation and the relative oil permeability (Koci et al., 1989). Wang et al. (2006) investigated the effect of oil viscosity on relative permeability curves for oil-water in sand packs. The measurements were made at constant flow rate. The decrease in oil viscosity was linked to an increase in both oil and water relative permeability curves (Wang et al., 2006).

The impact of temperature on oil-water relative permeability, interfacial tension, and wettability has been reviewed by (Esmaeili et al., 2019). Observations on the effect of temperature on two-phase flow in porous media were mainly linked to variations in those parameters. Therefore, it is very difficult to extend the findings from literature reviews on different liquids to a complex liquid such as coal tar. Also, some authors pointed out that a lot of relative permeability available data is not exact due to the presence of experimental artifacts, e.g. viscous fingering, capillary-end effects, wettability, and pore-distribution changes due to temperature variations. Specifically, reliable relative permeability measurements require a flow regime dominated by capillary forces at the pore scale.

Equation (1) is only valid for low capillary numbers (Davit and Quintard, 2019). Oil reservoirs generally have low permeability, less than 10^{-11} m^2. The velocity is generally low enough to validate the hypothesis behind the use of generalized Darcy's law. However, in the case of soil remediation, the NAPL phase is present due to a spill and is often found in highly permeable zones in the subsurface, above 10^{-11} m^2. For instance, in our application case, coal tar was pumped in alluvial sands with a permeability of 10^{-9} m^2.

The use of generalized Darcy's law and Eq (2) implies a quasi-static assumption. The interface between both fluid phases is described by a succession of quasi-static thermodynamic states,

without any dependence on time. Capillary effects are predominant at the pore scale and are represented at macroscale using Eq (2). Relative permeabilities represent viscous effects to generalize Darcy's law to multiphase flow. However, this assumption is not always satisfied when considering multiphase flows in a transient process. For instance, when considering pumping NAPL in the subsurface, the capillary number will be obviously very high near the production well.

The main objective of this work is to measure changes in the physical properties of coal tar caused by temperature variations and to relate those to two-phase flow properties in highly permeable porous media. We explored how temperature influences the capillary pressure-saturation and relative permeability curves under quasi-static two-phase flow conditions. Our goal was to better understand and characterize the two-phase flow in highly permeable porous media with a focus on temperature.

First, we determined the properties of coal tar sampled from a real polluted site (Section 2). Data on its density, dynamic viscosity, interfacial tension with water, and contact angle with water on a glass slide were measured between 293.15 K and 323.15 K. Then we describe an experimental setup that has been used to study two-phase flow in porous media in isothermal conditions (Section 3). We conducted experiments at two temperatures (293.15 K and 323.15 K) under quasi-static conditions. Then we carried out drainage and imbibition tests at different flow rates and temperatures to study the effect of temperature on two-phase flow under dynamic conditions. Finally, we summarize the results including the capillary pressure-saturation relationship, analysis of used dimensionless numbers, and a discussion on saturation and pressure time-profiles as well as relative permeability curves obtained under dynamic conditions (Section 4).

2. Fluid characterization as a function of temperature

2.1. Fluid selection and properties

The main couple of liquids for this study is coal tar and water. Coal tars are pyrolysis by-products. Polycyclic aromatic hydrocarbons (PAHs) are the main chemical compounds found in coal tars. Previous studies on coal tars indicate that their physical properties depend on their chemical origin and the geology of the source zones (Kong, 2004). In addition, the complete chemical composition of coal tars is hard to determine by analytical means (Johansson et al., 2019). We used a coal tar sample produced from a well situated in a former coke plant. Suspended solid particles were removed from the sample using a glass fiber membrane (GF/D, 2.7 µm pore size). Some water was also collected during coal tar sampling. The water contained inside the sample was filtered out with a vacuum pump and a 10 µm pore size hydrophobic PTFE membrane. The resulting sample, containing only coal tar, was kept in a cold room at 277.15 K to limit chemical reaction rates, evaporation, and variations in physical properties during the study. Degassed tap water was used in all coal tar and water flow in porous media experiments. Ultrapure water was also considered for the experiments but was not suitable because coal tar dissolves partially in it.

DNAPLs, like coal tar, are generally difficult to experiment with due to their high toxicity and their adhesion on laboratory glassware. As previously mentioned, coal tar has generally an unknown and very heterogeneous composition. It has also been observed that the composition of coal tar can change in the experimental setups. Therefore, we chose a model fluid pair made of two immiscible pure compounds, canola oil and ethanol. Virgin canola oil was used as the substitute for coal tar (non-wetting fluid). The choice of virgin oil was motivated by the fact that refined canola oil was found to change color when heated. Vegetable oils have however a lower density than water. Thus,

we chose to work with ethanol as the wetting fluid. Sodium chloride was dissolved into the ethanol at room temperature (293.15 K) at a concentration of 0.65 g/kg. The addition of salt was required to measure soil resistivity in a parallel study (Iravani et al., 2020). From this point, water and salty ethanol will be referred to as the wetting phase. Coal tar and canola oil will be referred to as the non-wetting phase.

2.2. Density

We measured all the densities (coal tar, water, salty ethanol, canola oil) using a pycnometer (25 mL ± 0.04 mL) and an analytical balance (± 0.01 g). The pycnometer was first calibrated with ultrapure water at room temperature (293.15 K). Density values were then measured at the same temperature. The effect of temperature on density was determined by placing the liquid inside an insulated closet initially at 293.15 K. The temperature of the closet was increased by steps of 10 K and the density was then measured with the same pycnometer. The procedure was repeated until reaching 323.15 K in triplicate per liquid. Finally, measurements were also acquired at 277.15 K by placing the sample in a cold room.

Figure 1 presents the density measurements as a function of temperature for ethanol, canola oil, water, and coal tar. Coal tar has a higher density than water at all temperatures tested in this study. Therefore, coal tar behaves as a DNAPL in the polluted aquifer zone. The coal tar density values measured in this study were close to previously reported measurements at 295.15 K, 308.15 K, and 323.15 K (Kong, 2004).

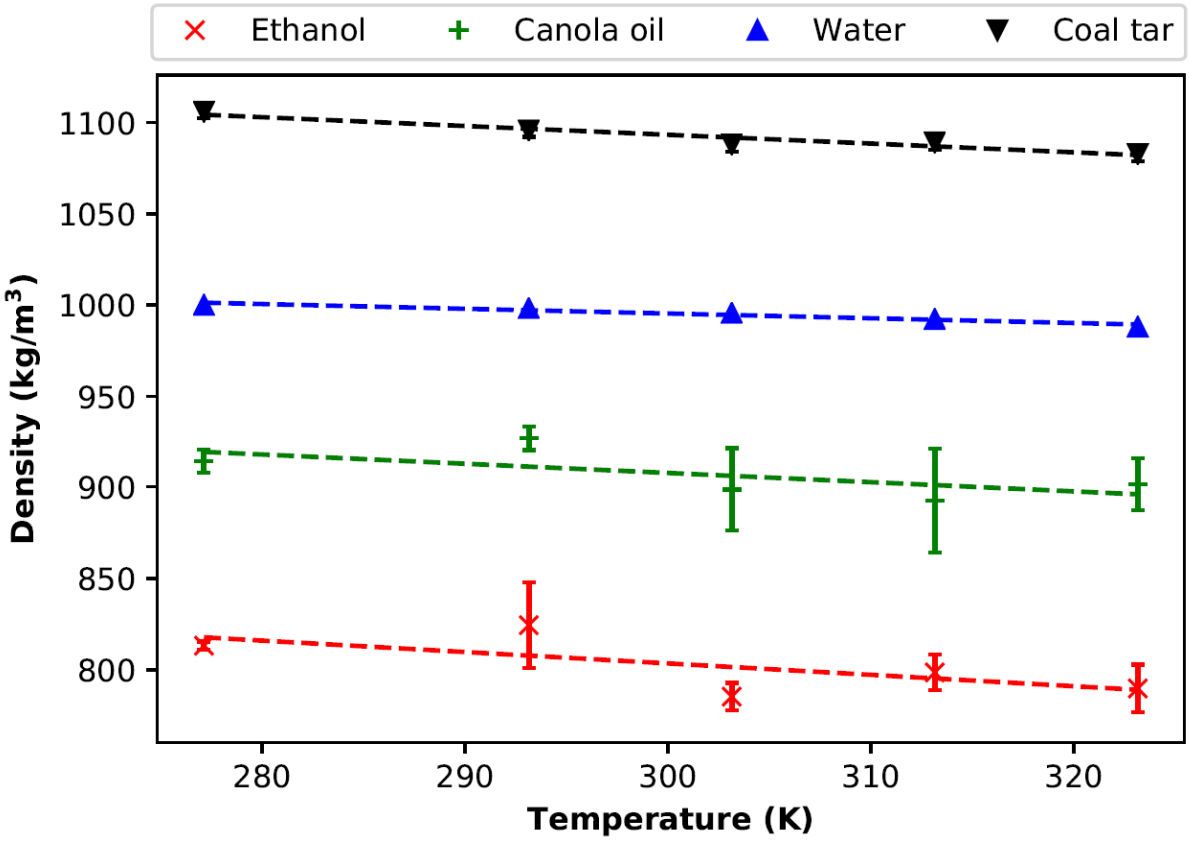

Figure 1: Changes in canola oil, salty ethanol, water, and coal tar densities between 277.15 K and 323.15 K

Linear regression was applied using the least-squares method. We observed that ethanol, canola oil, water, and coal tar densities decrease almost linearly when their temperature increases from 277.15 K to 323.15 K. The measurements indicate that the volumetric thermal expansion coefficient can be considered constant for these fluids. For each fluid, the estimated correlations are the following, with temperature in Kelvin:

$$\rho_{CT}(T) = 1237 - 0.4818\,T \quad (6)$$

$$\rho_{W}(T) = 1073 - 0.2598\,T \quad (7)$$

$$\rho_{E}(T) = 990.3 - 0.6224\,T \quad (8)$$

$$\rho_{O}(T) = 1059 - 0.5033\,T \quad (9)$$

2.3. Dynamic viscosity

We measured all the dynamic viscosities (coal tar, water, salty ethanol, canola oil) using a rotational rheometer (Thermo Scientific Haake™ Mars™ III) and cone-plate geometry. The plate was connected to thermoelectric cooling (Peltier effect) in order to reach temperatures between 283.15 K and 323.15 K. The rheometer applied a constant shear rate and measured the responding shear stress of the liquid. Correct calibration of the gap between the cone and the plate is of great importance for precise measurements. In our study, this gap can change due to thermal expansion. Thus, we first heated the plate to the desired temperature then calibrated the gap prior to measurements. Finally, the liquid sample (2 mL) was injected onto the plate. The range of the shear rate measurements was comprised between 10 s^{-1} and 100 s^{-1}. For Newtonian fluids, the shear stress is proportional to the shear rate. In this case, the dynamic viscosity μ is defined as a constant proportionality factor between both parameters.

First, coal tar shear stress was determined at 293.15 K for shear rates varying from 10 s^{-1} to 100 s^{-1}. The shear stress increased proportionally as the shear rate increases. Thus, the coal tar sampled in this study displays the behavior of a Newtonian fluid between 283.15 K and 323.15 K. Previous studies have found that liquid coal tar is shear thinning (Bhatia et al., 1977; Fitzer et al., 1987). The difference in behavior found here may be due to either the historical origin of the coal tar sample or the focus on a lower temperature (283.15 K) compared to these studies (> 373.15 K). Figure 2 presents the effect of temperature on the dynamic viscosities of ethanol, canola oil, water, and coal tar. Dynamic viscosities decreased while temperature increased in all fluids The Andrade equation (two parameters empirical exponential model) was used to fit viscosity data (Andrade, 1940). The relative changes of dynamic viscosity due to temperature were found to be close for non-wetting liquids (canola oil and coal tar) and also wetting liquids (ethanol and water).

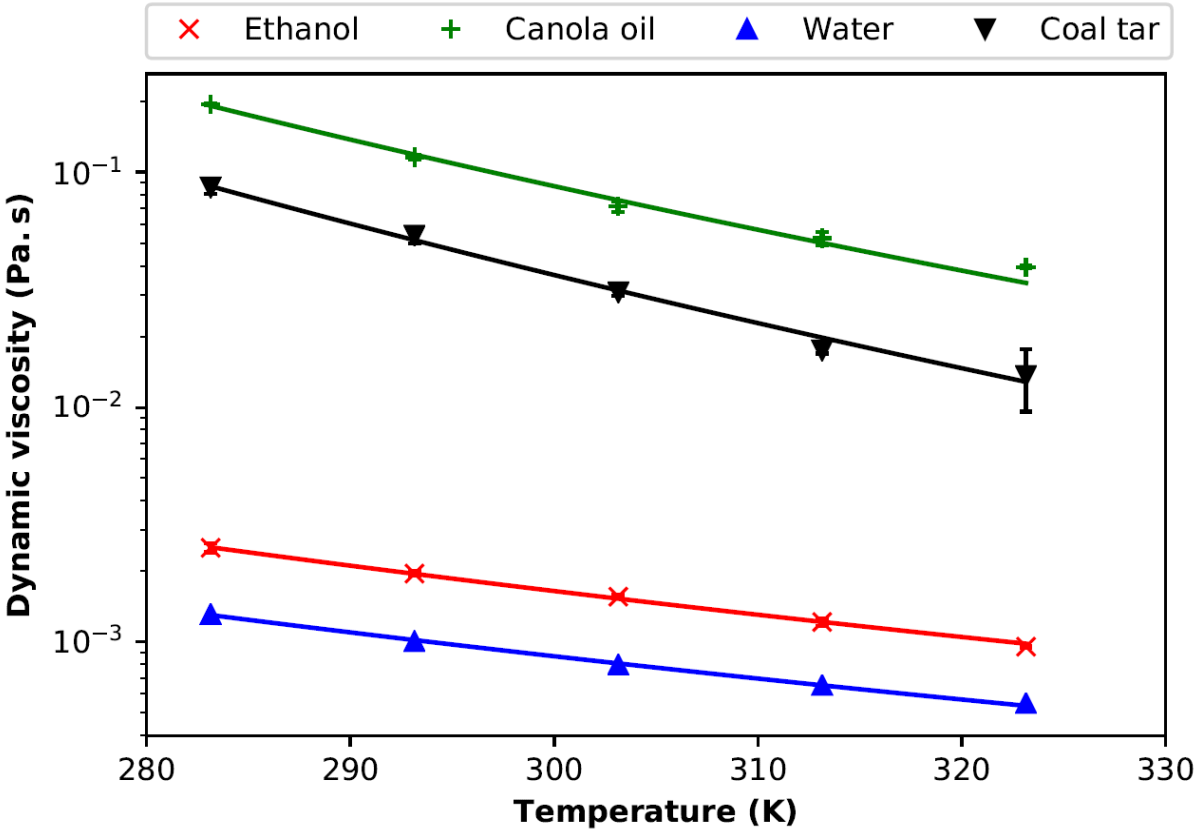

Figure 2: Dynamic viscosity of salty ethanol, canola oil, water, and coal tar as a function of temperature. Lines represent data fitting with Andrade two-parameter exponential function

$$\mu_{CT}(T) = 1.71 \times 10^{-8}\, e^{\frac{4.37\times10^{3}}{T}} \quad (10)$$

$$\mu_{W}(T) = 9.82 \times 10^{-7}\, e^{\frac{2.03\times10^{3}}{T}} \quad (11)$$

$$\mu_{E}(T) = 1.22 \times 10^{-6}\, e^{\frac{2.16\times10^{3}}{T}} \quad (12)$$

$$\mu_{O}(T) = 1.60 \times 10^{-7}\, e^{\frac{3.96\times10^{3}}{T}} \quad (13)$$

2.4. Interfacial tension and contact angle

Interfacial tension and contact angles measurements were made with a drop shape analyzer (Krüss DSA 100). The apparatus consists of a light source, a camera, and the sample provided by a syringe. A drop of the non-wetting fluid (coal tar or canola oil) is injected into a bath filled with the wetting fluid (water or salty ethanol). The bath and the syringe are surrounded by an insulated chamber. The chamber is connected to a thermostat, which can change the measuring temperature between 285.15 K and 323.15 K. The accuracy for interfacial tension, contact angle, and temperature measurements are respectively 0.3 mN/m, 0.3°, and 0.1 K. A camera, controlled by Krüss ADVANCE

software is able to detect the drop and shape contours from images for interfacial tension and contact angle measurements.

The calibration of the apparatus was checked by measuring pure water's surface tension between 285.15 K and 323.15 K. For interfacial tension measurements, a 1 mm diameter PTFE needle was used. A non-wetting drop was formed at the tip of the needle directly inside the wetting fluid. The choices of needle diameter and drop volume were motivated by a previous work (Berry et al., 2015). The measurements were done in triplicate for each target temperature. The measurements were then acquired every minute and averaged over one hour. The interfacial tension was determined with Young-Laplace equation. The method used by Krüss ADVANCE software automatically detects the drop in the image and fit shape factor in order to reproduce its contour. The interfacial tension is then calculated from:

$$\gamma = \Delta\rho g \frac{R_0^2}{\beta} \qquad (14)$$

where $\Delta\rho$ is the difference between densities of the two phases, g the standard acceleration due to gravity, R_0 the drop radius at its apex, β a shape factor.

For contact angle measurements, a glass slide was introduced inside the wetting fluid (water and ethanol) bath. A non-wetting fluid (DNAPL and canola oil) drop was then injected on the glass slide. The drop shape was reproduced by Krüss software using the previously introduced Young-Laplace equation. The contact angle was measured as the angle between the detected contour and baseline, represented by the horizontal glass slide. Pure water-air surface tension measurements were in agreement with previous ones made by (Vargaftik, 1983). This validates the proposed experimental apparatus and our protocol.

Prior to temperature measurements, interfacial tension was measured against time for a coal tar/tap water system over 200 minutes at 293.15 K and 323.15 K. The interfacial tension decreased in both cases as coal tar ages in tap water. This change in interfacial tension results from a small amount of coal tar dissolving rate into the water at the interface. The measurements could not be taken for a longer time as the drop fell off afterwards. To discuss only the temperature effect, all the interfacial tension measurements that follow were taken after 2 minutes.

The interfacial tension measurements for salty ethanol/canola oil and coal tar/water are plotted in Figure 3.

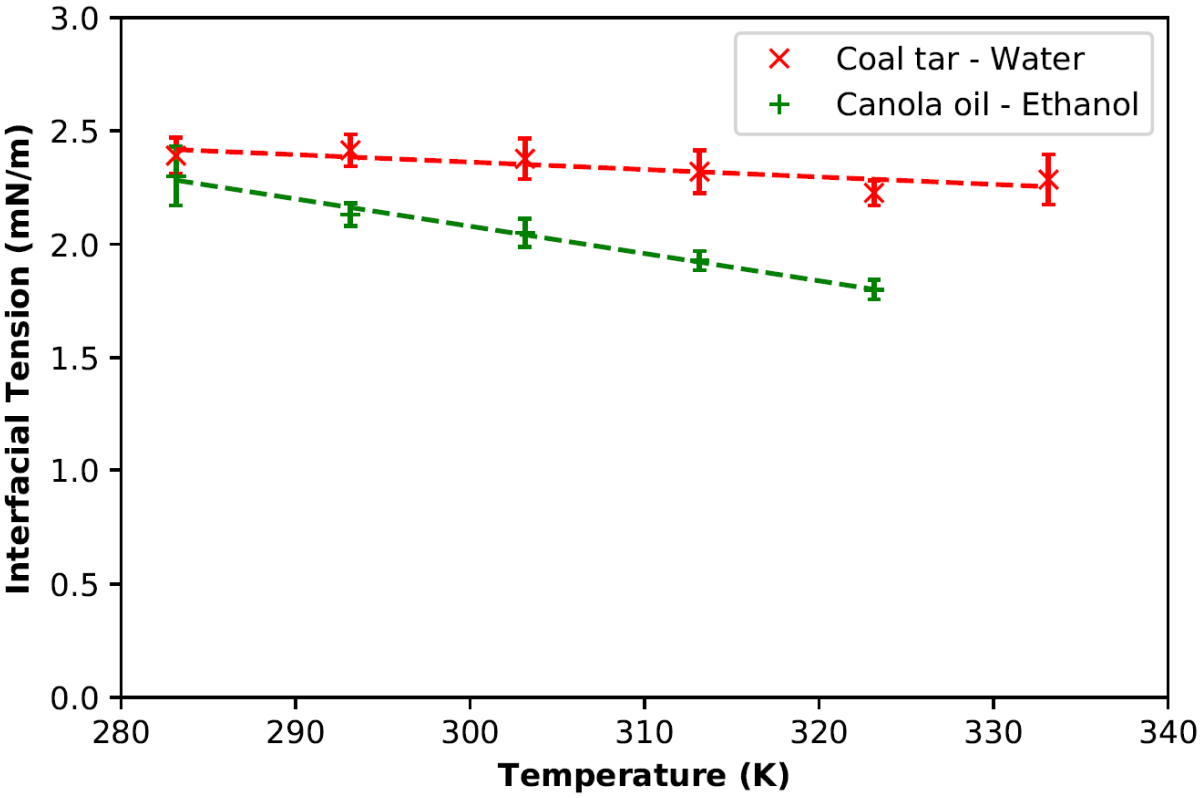

Figure 3: Interfacial tension of canola oil/ethanol and coal tar/water as a function of temperature

The reported range of interfacial tensions is generally comprised between 20-50 mN/m for TCE, PCE, and chlorinated solvents with water at 293.15 K (Cai and Mohanty, 1997; Dawson and Roberts, 1997; Smith and Zhang, 2001). Yet, for both fluid pairs studied, we observed low interfacial tensions (< 3 mN/m). Such low values are found for liquids containing amphiphilic substances. This may be the case for the coal tar used in this study as it was a mixture sampled from a real polluted site and its exact chemical composition is unknown. Commercial oils can also contain additives that reduce the interfacial tension of water/oil (Gaonkar, 1989). Sanaiotti et al. (2010) measured a range of interfacial tensions between soybean oil and water and ethanol mixtures (Sanaiotti et al., 2010). The reported values were between 1-3 mN/m, which are close to what we measured. Unknown additives inside the oil might be the cause of these differences.

Previous studies have found that the influence of temperature on interfacial tension is linked to its influence on mutual solubility. For binary mixtures composed of a polar and a non-polar liquid, solubility increases linearly with temperature. As a consequence, interfacial tension also decreases linearly (Donahue and Bartell, 1952). The same trend was found here for coal tar and water, as well as for canola oil/ethanol in our measurements. However, the decreasing interfacial tension with temperature for canola oil/ethanol was more significant than the decrease for the coal tar/water system. The linear relationships between interfacial tension and temperatures for both fluid pairs are described by:

$$\gamma_{CT/W}(T) = 3.3 - 3.3 \times 10^{-3} T \quad (15)$$

$$\gamma_{O/E}(T) = 5.7 - 1.2 \times 10^{-2} T \quad (16)$$

The accuracy of the apparatus was 0.3 mN/m, which is around 10 % of our absolute measurement value.

Figure 4 presents contact angles for coal tar and canola oil droplets against temperature. The variations of contact angle are not significant between 283.15 K and 333.15 K and can be considered constant with temperature. The slight variations observed on coal tar sessile drops could also be due to repeatability issues with the sessile drop method. All materials were cleaned thoroughly between any two measurements and the measurement conditions (temperature, injection speed, and droplet size) were precisely respected.

The measured contact angles between both couples of liquids seem close. However, coal tar also sticks on solid surfaces while canola oil does not. Our measurements of contact angle on a glass slide are a first indication of wetting phase conditions. They do not reflect the more complex behavior happening with complex liquids, like coal tar, inside a real porous medium.

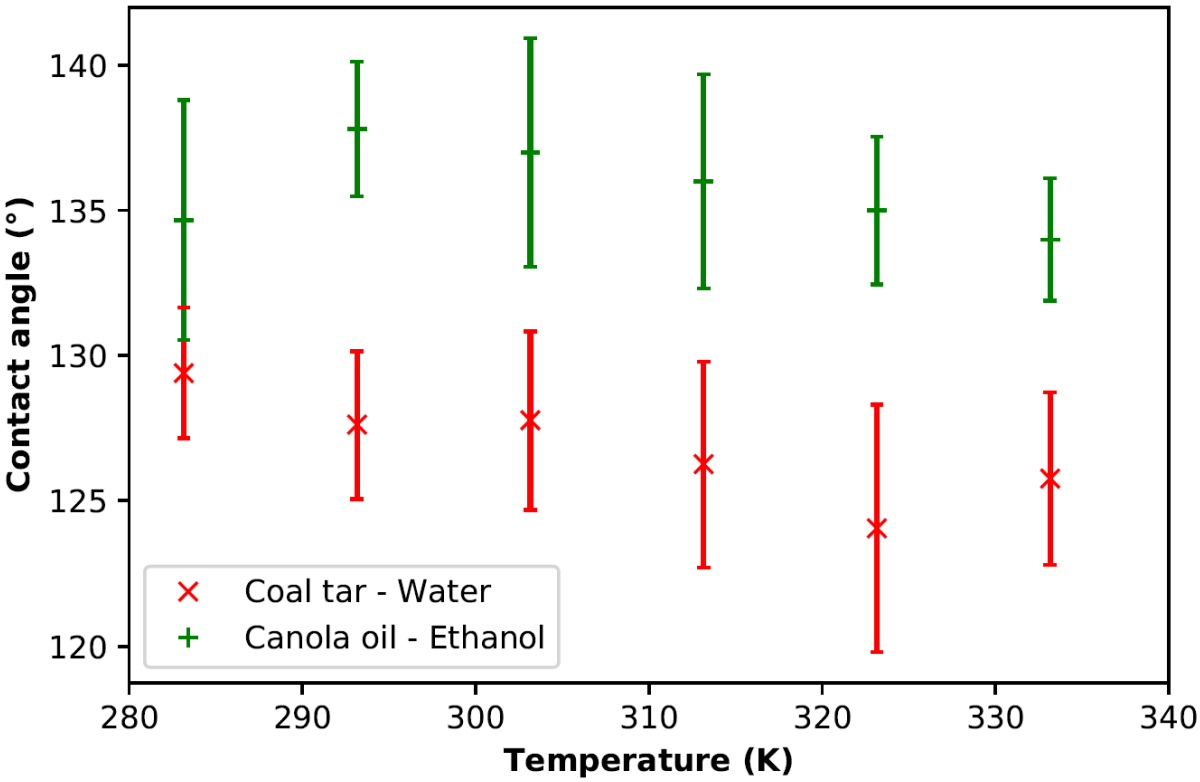

Figure 4: Evolution of coal tar/water and canola oil/ethanol contact angle on a glass slide

3. Experimental setups and procedures for capillary behavior characterizations

The parameters measured in Section 2 indicate that temperature has an effect only on the dynamic viscosities of the fluids. Here we performed the drainage and imbibition experiments for coal tar/water and canola oil/ethanol in two experimental configurations (Figure 5). First, small pressure variations were applied using a small 1D column to limit viscous fingering and measure capillary pressure-saturation curves at 293.15 K and 323.15 K. This also avoided interface instability. Thus, we

focused on how parameters change with temperature in a generalized Darcy's law application case. The drainage and imbibition experiments were done using a small transparent 2D cell using the same configuration as before. Finally, the 2D cell was connected to a volumetric pump where flow rate and temperature were varied to observe their effects on saturation and pressure profiles.

3.1. Experimental setups

Experiments were carried out inside a 1D vertical column (diameter 5.2 cm, height 5.6 cm). The column (Figure 5a) was made of polyvinylidene fluoride (PVDF) to resist coal tar corrosion. The measurements were made for both fluid pairs: coal tar/water and canola oil/ethanol. Coal tar was sampled from a field mainly composed of coarse sand with d_{50} = 1 mm. Thus, 1 mm homogeneous glass beads were chosen for the experiments. This was to avoid inaccuracies due to adsorption effects, particle shape heterogeneity, pore-size distribution, and possible wettability changes during data acquisition. As shown in Figure 5b, the drainage-imbibition experiments for coal tar/water and canola oil/ethanol were also performed in a small 2D cell (length = 5.0 cm, height = 5.0 cm, width = 2.0 cm). This 2D cell was also made of PVDF to ensure high corrosion resistance against coal tar. The cell was made of two transparent glass plates in order to visualize the two-phase flow using imaging. The container with both fluids was placed on a Sartorius Cubis MSE (± 0.1 g) mass scale acquiring data automatically every 6 s. Two pressure transducers (KELLER PR33X, ±300 Pa) were added to the setup as three-way junctions at the top and bottom of the cell. The tubing connected to transducers was filled with ethanol initially to avoid the presence of air in the system. Both transducers were initially calibrated to read 0±10 Pa at atmospheric pressure at their respective positions.

The homogeneity of our beads was checked with sieves with mesh sizes between 0.96 mm and 1.04 mm. The mass of glass beads inside the medium was kept constant in order to ensure similar compaction, porosity, and initial saturation between various experiments. The column was filled with glass beads and vibrated slowly during the packing process. Glass beads were held inside the setup using the stainless-steel grids (mesh size 0.9 mm).

Initially, the wetting phase was injected at 25 mL/min with a peristaltic pump inside the porous medium. The possible presence of residual air was checked by measuring porosity and permeability. Experiments were conducted on columns with a porosity between 0.39 and 0.42. The mean permeability of the glass beads was measured to be 3.5×10^{-10} m^2.

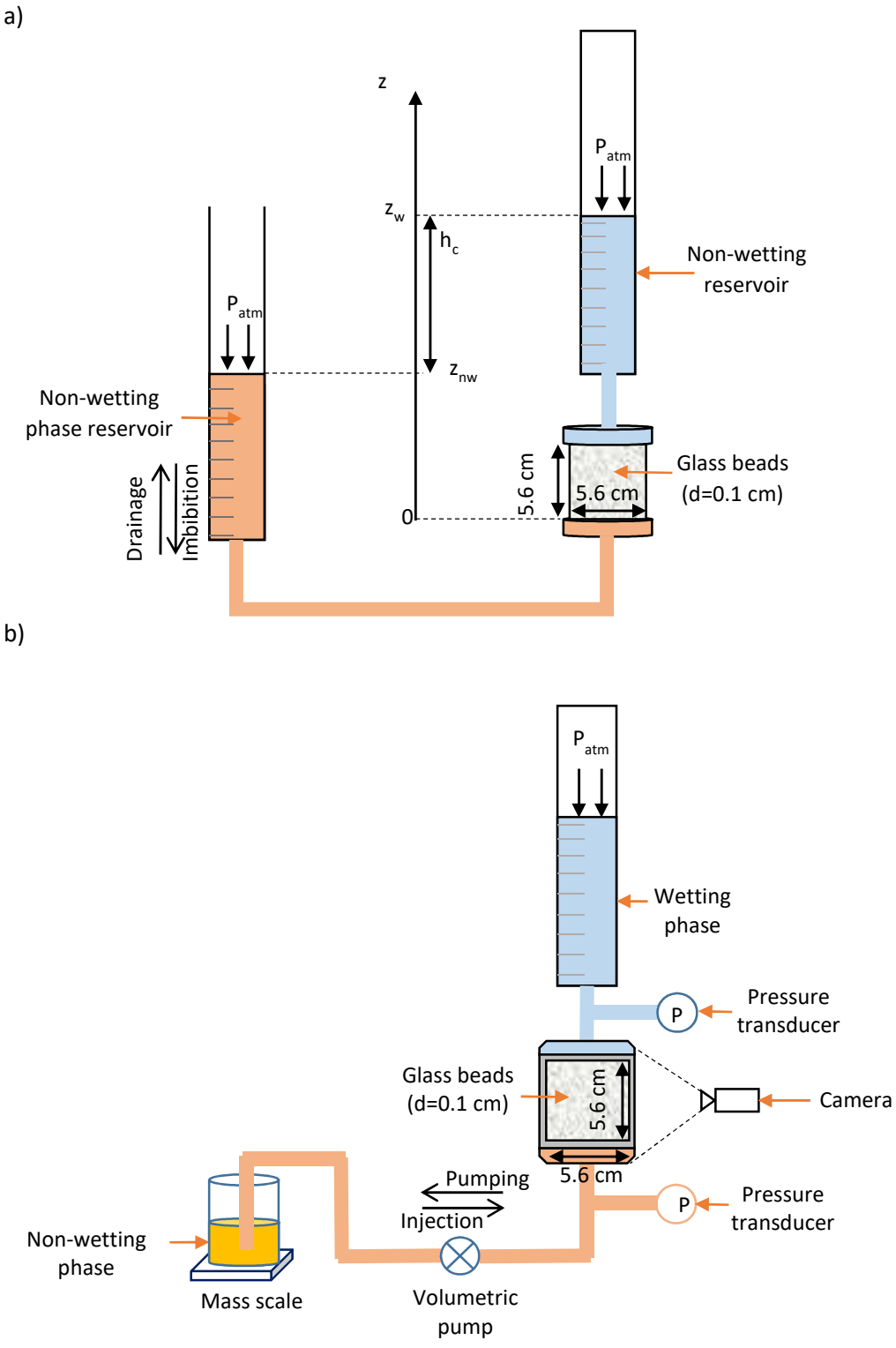

Figure 5: Drainage/Imbibition setups used for (a) capillary pressure-saturation measurements and (b) setup used for experiments in dynamic conditions

3.2. Quasi-static experiment procedure

In the quasi-static experiment setup, the column was connected to two scaled reservoirs (3.5 cm internal diameter and 41.8 cm high). Details on the experimental setup in quasi-static conditions are available in (Colombano et al., 2020). One reservoir was connected to the bottom of the column and filled with the non-wetting phase. The other reservoir was connected to the top and filled with the wetting-phase. In this setup, the measurements were made by successive equilibrium states. The capillary pressure p_c is defined as the difference between the pressure of the non-wetting phase and that of the wetting phase. Thus, the capillary pressure can be directly defined as the difference of hydrostatic pressures h_c between the non-wetting and wetting liquids.

$$p_c = p_{nw} - p_w = (\rho_{nw} - \rho_w) g h_c \qquad (17)$$

We chose the initial conditions for the experiments so that the interface between the non-wetting and wetting phase would be at equilibrium at the bottom of the 1D column. This means that $z = 0$ () corresponds to a level of non-wetting fluid z_{nw} equal to $\rho_w z_w / \rho_{nw}$. For drainage experiments, the non-wetting reservoir base level was progressively increased by $z = 0.02$ m steps, which represents 20 Pa and 18 Pa variations at 293.15 K and 323.15 K respectively. The volume balance between the non-wetting phase level z_{nw} and wetting phase level z_w gave the saturation change between two successive steps. This process was repeated until no difference could be observed between the non-wetting and wetting reservoir volume variations. The levels of non-wetting and wetting fluids could be determined with a precision of 1 mm. The irreducible wetting saturation $S_{ir,w}$ was measured as the difference between initial and produced volumes of the wetting phase reservoir during drainage. For imbibition experiments, the non-wetting phase reservoir base level was decreased by 0.02 m steps. This time, the difference between the initially injected non-wetting phase volume and the volume produced during the imbibition gave the residual non-wetting saturation $S_{r,nw}$.

The time step between each height change is an important parameter for achieving the equilibrium condition. This time step was kept constant for experimental repeatability. To choose this time step, we measured the level of the interface inside the 1D cell after a 0.02 m step. This level was stationary 3 hours after changing the non-wetting phase reservoir for coal tar/water, and 1 hour for oil/ethanol during imbibition. We saw slightly low stabilization times during drainages. This is mainly due to the influence of gravity (drainages are produced upwards, imbibitions downwards). Hence, the reservoir level was changed when the saturation in the cell was constant. These experimental conditions have been chosen in order to keep a capillary dominant process inside the cell.

The heights measurements were corrected for the evaporation rate, using a reference reservoir to quantify water level change because of evaporation. Also, we limited evaporation by closing the end of the reservoirs with a perforated plastic cap. As pointed out before, the reservoirs were made with PVDF which is hydrophobic. Therefore, the volume attached to the reservoir wall is not significant and was not considered for hydrostatic pressure measurement.

For canola oil/ethanol and coal tar/water, two sets of three cell experiments were carried out at 293.15 K and 323.15 K. The whole setup was placed in an oven when heated at 323.15 K. Each set consisted of two successive drainages and imbibitions. For the first set of experiments, the temperature was kept at 293.15 K for the whole experiment. For the second set, the primary drainage was performed at 293.15 K but the temperature was increased to 323.15 K from the first imbibition.

For each experimental case, capillary pressure versus saturation datasets were fitted on van Genuchten empirical model using a Levenberg-Marquardt Algorithm (LMA) written in Python.

$$S_w = S_{ir,w} + \frac{1 - S_{ir,w} - S_{r,nw}}{(1 + (\alpha h_c)^n)^{1-\frac{1}{n}}} \quad (18)$$

We found that this model gave the best least-squares residuals out of all tested for our data. Van Genuchten parameters (α,n) and residual saturations have been averaged for each experiment.

3.3. Dynamic pumping experiment procedure

In this case, the drainage and imbibition experiments were done only for the oil/ethanol system as coal tar was completely opaque and the imaging procedure was not suitable for determining coal tar saturation inside the cell.

For both drainage and imbibition, we used three constant flow rates at room temperature (6, 12, 24 mL/min at 293.15 K) in a clockwise motion. After injecting 2 pore volumes, the pump's direction of rotation was changed to recover the non-wetting phase (imbibition). Oil/ethanol imbibition was also carried out at 12 mL/min at 323.15 K to study the effect of temperature.

Figure 6 presents photographs of the cell during the dynamic experiments. The interface between salty ethanol and canola oil observed during drainages was stable for all cases. Only two pore volumes were needed to reach irreducible ethanol saturation. However, imbibitions were unstable and prone to viscous fingering. Ten pore volumes were pumped during imbibition.

In all cases, the pressure difference initially increased because of the ethanol injection until a value of 3800 Pa. The pressure was read every 6 seconds. We observed substantial oscillations on the pressure readings due to the pump's peristaltic motion. A digital low-pass filter with a cut-frequency equal to the cycle frequency of the pump was applied to the data to remove these artefacts.

The sum of the wetting and non-wetting phase outlet masses was measured continuously during the experiment. The mass was measured every 6 seconds during both drainage and imbibition.

a) Injection of oil from the bottom (293.15 K, 12 mL/min)

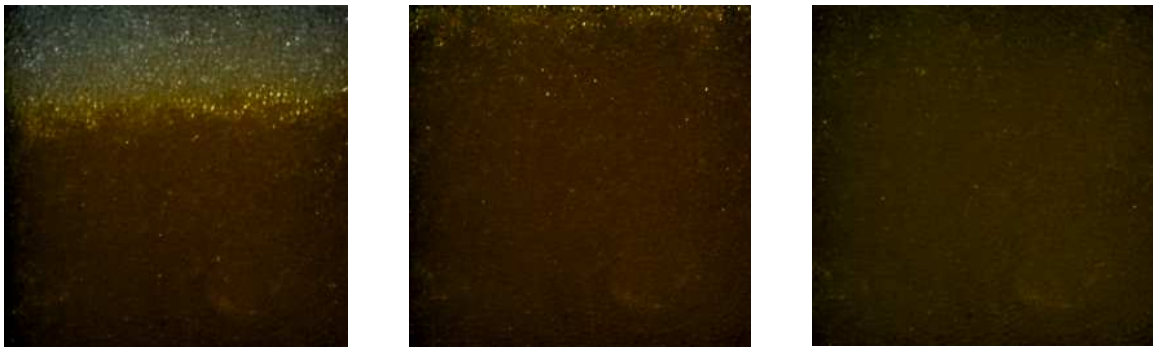

b) Pumping of oil from the bottom (293.15 K, 6 mL/min)

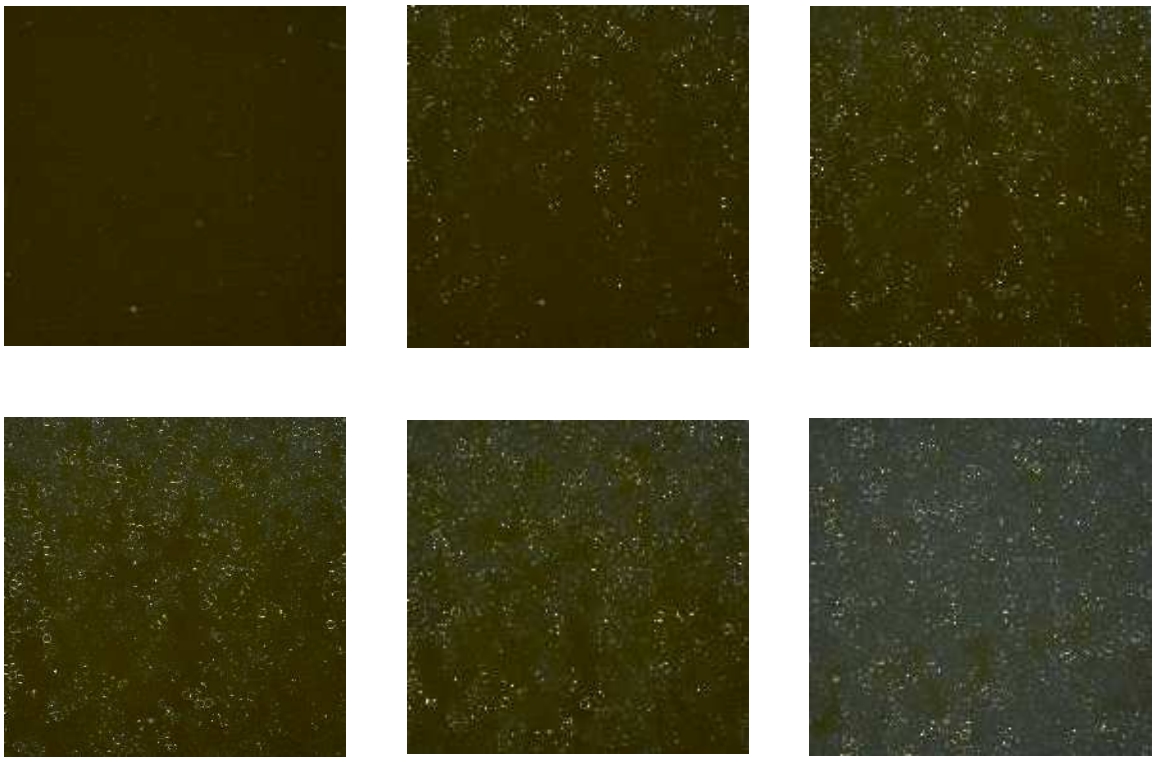

Figure 6: Images taken during (a) injection at 12 mL/min and (b) pumping at 6 mL/min of oil inside 1 mm glass beads initially saturated with ethanol. As oil is being injected, a sharp horizontal interface is being pushed in. On the contrary, when oil is being pumped, viscous fingers appear and trap the oil ganglia

3.4. Saturation measurements using imaging

Saturation was determined inside the 2D small cell with an imaging technique. A Nikon® D810 with NIKKOR LENS 105 (Nikon®) digital camera which has a 34 megapixel resolution was used for optical imaging. Images were acquired every 30 seconds during the injection or pumping of the non-wetting phase. The experiments were performed in a dark room with two light spots (2×300 W, Broncolor®). Camera parameters and lighting conditions were identical for all experiments. Light transmission and light reflection methods have both been used in the past to observe two-phase flow processes in porous media (Geel and Sykes, 1994; Darnault et al., 1998; Wu et al., 2017). In this study, the light reflection method (LRM) was used. The main idea of imaging analysis is to determine a relationship between light intensity and wetting-phase saturation S_w. Previous work found an exponential relationship between light intensity and saturation (Gerhard and Kueper, 2003; Colombano et al.,

2020). The images were in RGB but were transformed in 8-bit images for image analysis. The mean gray values were obtained using Fiji freeware. The following procedure was applied for image analysis of photos from the same experiments:

- Adjust or correct lighting differences with the 8-grayscale levels. The black and white square correspond to the reflectance of 18.9% and 98.2% respectively as reference values.
- Determine the pixel area to be analyzed. The pixel area has to be big enough to avoid microscale effects, but at the same time not too big to avoid shadows and non-uniform lighting. The mean gray value averaged over the pixel area was plotted before analyzing images. This plot was used to determine an area where the mean gray value was constant.
- Use a calibration curve to determine the wetting phase saturation inside the cell. For the calibration, we took images of cells containing a known volume fraction of glass beads and liquids.

For each saturation endpoints ($S_w=S_{ir,w}$ or $S_w=1-S_{r,nw}$), the cell was uniformly saturated and the reflected light intensity was measured (Fig B.1). The optical density was defined as the ratio between this measured intensity and the intensity of a white reference (98.2%).

For oil and ethanol, we found a linear relationship $S_w = -2.63\ OD + 2.34$ with a coefficient of determination R^2 close to 1 (R^2 = 0.95). This result means ethanol saturation can be determined directly from light intensity measurements. This property is useful in order for measuring saturation, especially in dynamic conditions.

For both fluid pairs, the relationship between optical density and saturation was measured at 293.15 K and 323.15 K. We saw no effect of temperature on the relationship between optical density and saturation.

4. Results & Discussion

4.1. Effect of temperature on quasi-static capillary pressure-saturation curves

An example of the capillary pressure-saturation curves is plotted in Figure 7 at 293.15 K for coal tar/water. The experimental data from all three experiments are presented by crosses (exp) without distinction. However, van Genuchten parameters were obtained for each experiment separately and then were averaged (solid and dashed lines). Fitted van Genuchten parameters, irreducible and residual saturations are summarized in Table 1 for all experiments. This model uses two fitting parameters: α (m^{-1}) and n, which are related to the inverse of the entry pressure and the homogeneity of the porous medium, respectively. For oil/ethanol and coal tar/water experiments, α values are different. This result is coherent because their corresponding measured values of interfacial tension are not the same. The parameter n is also much higher for coal tar/water than for oil/ethanol. Wetting irreducible and non-wetting residual saturations are almost the same when comparing the same case for both fluid pairs. Following (Dury et al., 1998), we also calculated β coefficients (Table 1), the ratio between the inverse of α and the interfacial tension, for all experiments. This ratio is used to scale existing capillary curves to other fluid pairs. In our case, we found that the values are slightly higher for oil/ethanol than coal tar/water. Thus, using the scaling procedure, it is not possible to get coal tar/water capillary pressure-saturation curves from

oil/ethanol ones. Our results indicate that the scaling laws are not suitable when using complex fluids like coal tar.

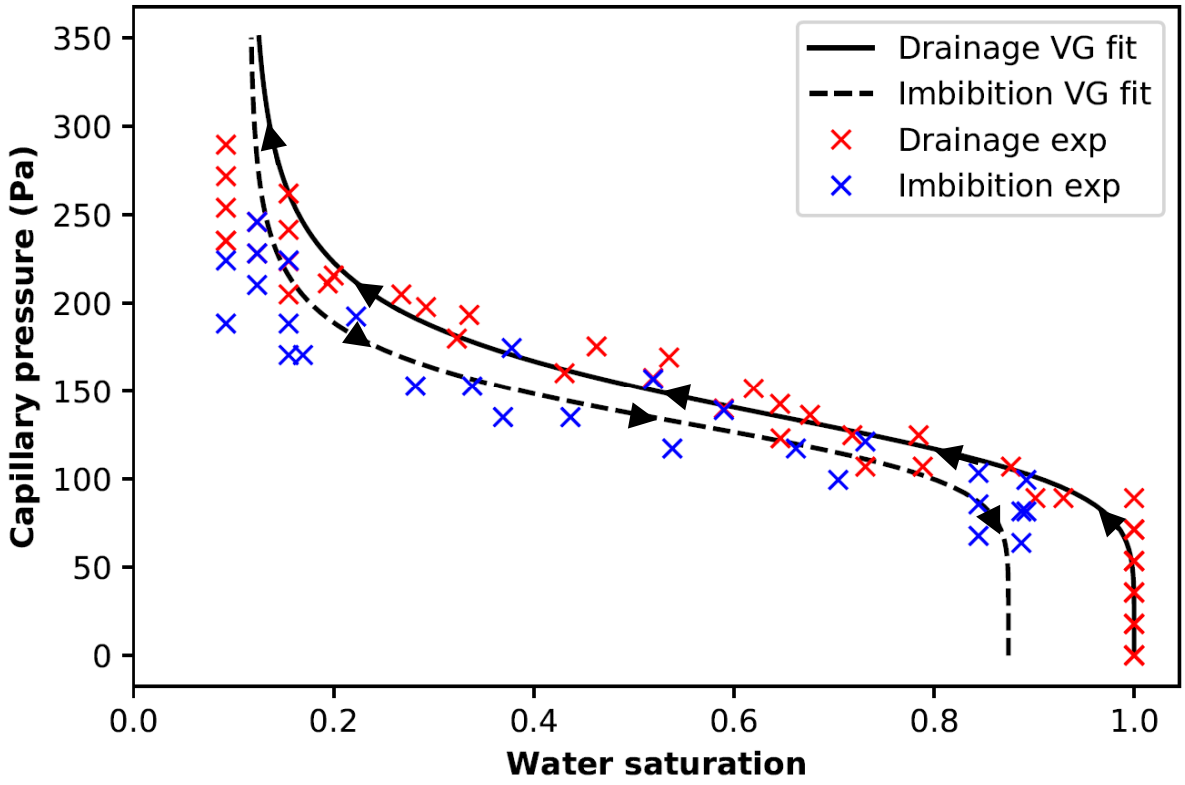

Figure 7: Data from triplicates experiments and averaged fitted capillary pressure-water saturation curves at 293.15 K for coal tar/water (primary drainage)

Table 1: Summary of all drainage-imbibition experiments in the 1D cell

Fluids	T (K)	Step	α (m^{-1})	n	$S_{ir,w}$	$S_{r,o}$	β
Oil/Ethanol	293.15	Drainage 1	5.52±0.22	3.17±0.58	0.10±0.02	0	0.085
Oil/Ethanol	293.15	Imbibition 1	4.90±0.30	3.57±0.45	0.10±0.02	0.14±0.02	0.096
Oil/Ethanol	293.15	Drainage 2	4.03±0.39	4.19±0.31	0.13±0.03	0.14±0.02	0.116
Oil/Ethanol	293.15	Imbibition 2	4.22±0.52	4.16±0.35	0.13±0.03	0.15±0.02	0.111
Oil/Ethanol	293.15	Drainage 1	6.22±0.43	2.96±0.50	0.11±0.02	0	0.075
Oil/Ethanol	323.15	Imbibition 1	5.34±0.45	3.09±0.38	0.11±0.02	0.13±0.03	0.104
Oil/Ethanol	323.15	Drainage 2	4.17±0.27	3.89±0.25	0.14±0.04	0.13±0.03	0.133
Oil/Ethanol	323.15	Imbibition 2	4.11±0.48	4.10±0.42	0.14±0.04	0.15±0.04	0;135
Coal tar/Water	293.15	Drainage 1	7.19±0.25	5.87±0.99	0.12±0.03	0	0.058
Coal tar/Water	293.15	Imbibition 1	6.26±0.68	10.1±1.94	0.12±0.03	0.13±0.02	0.066
Coal tar/Water	293.15	Drainage 2	5.18±0.44	9.86±1.33	0.17±0.05	0.13±0.02	0.080
Coal tar/Water	293.15	Imbibition 2	5.53±0.50	12.1±2.29	0.17±0.05	0.16±0.03	0.075
Coal tar/Water	293.15	Drainage 1	8.20±1.0	6.58±0.67	0.11±0.05	0	0.051
Coal tar/Water	323.15	Imbibition 1	8.56±1.1	8.46±0.69	0.11±0.05	0.12±0.03	0.052
Coal tar/Water	323.15	Drainage 2	7.88±0.67	7.84±0.57	0.14±0.03	0.12±0.03	0.057
Coal tar/Water	323.15	Imbibition 2	7.96±0.83	9.67±1.09	0.14±0.03	0.14±0.03	0.056

For canola oil/ethanol and coal tar/water, the differences observed in capillary pressure-saturation curves between 293.15 K and 323.15 K are within the standard deviation and could not be attributed to temperature effect (Figure 8). However, for coal tar/water and the same water saturation values, the capillary pressure is lower at 323.15 K than at 293.15 K. The previous measurements indicate that temperature changes are almost negligible for density, interfacial tension and contact angle between 293.15 K and 323.15 K.

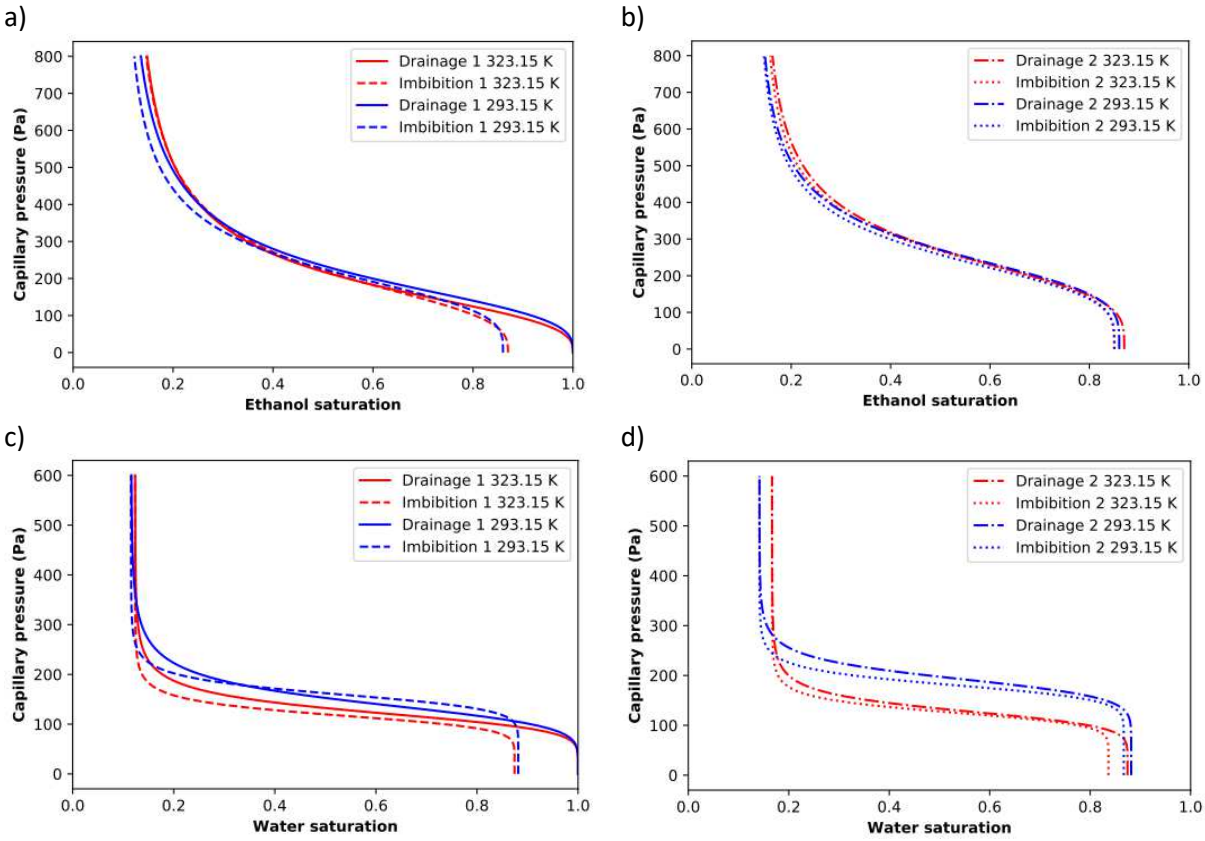

Figure 8: Effect of temperature on capillary pressure-saturation curves for a) oil/ethanol primary curves, b) oil/ethanol main curves, c) coal tar/water primary curves, d) coal tar/water main curves

We showed before that only dynamic viscosity was influenced by temperature changes. However, the dependency of the dynamic viscosity on temperature did not influence the capillary pressure-saturation curves in static conditions. The small difference between coal tar/water curves at 293.15 K and 323.15 K might be explained by either the heterogeneity of coal tar or alteration of the coal tar/water mixture at a higher temperature.

Density, dynamic viscosity, interfacial tension, and contact angle results were used to calculate the relevant dimensionless numbers related to imbibition experiments (Table 2). Bond number, Bo, and viscosity ratio, M, could be calculated directly with the measured parameters. The intrinsic velocity calculated with Darcy law was used to calculate Ca numbers. The pressure difference used in this expression is the same as the one used in our experiments. The resulting definition for Ca is thus equivalent to the one proposed in (Chatzis and Morrow, 1984). Since drainage is mostly a stable process due to a favorable viscosity ratio, dimensionless numbers will be calculated in the case of imbibition, to verify the validity of Darcy's law.

Table 2: Bond, capillary numbers and viscosity ratio associated with the two-phase flow of oil/ethanol and coal tar/water between 293.15 K and 323.15 K

Liquids	Coal tar – water			Canola oil - ethanol		
T (K)	Bo	Ca	M	Bo	Ca	M
283.15	4.19×10^{-1}	5.24×10^{-5}	1.48×10^{-2}	4.36×10^{-1}	5.46×10^{-5}	1.32×10^{-2}
293.15	4.16×10^{-1}	5.20×10^{-5}	1.96×10^{-2}	4.66×10^{-1}	5.82×10^{-5}	1.64×10^{-2}
303.15	4.13×10^{-1}	5.16×10^{-5}	2.55×10^{-2}	4.99×10^{-1}	6.23×10^{-5}	2.01×10^{-2}
313.15	4.09×10^{-1}	5.11×10^{-5}	3.26×10^{-2}	5.35×10^{-1}	6.69×10^{-5}	2.43×10^{-2}
323.15	4.05×10^{-1}	5.07×10^{-5}	4.11×10^{-2}	5.77×10^{-1}	7.21×10^{-5}	2.91×10^{-2}

We found the bond number to be slightly below 1 due to the small difference in density between the two phases. The flow between coal tar/water and oil/ethanol in 1 mm glass beads can, therefore, be described by Darcy's law. Oil/ethanol Bond number increases with temperature while that of coal tar/water decreases. This can be explained by the fact that the density difference $(\rho_{nw} - \rho_w)$ increases with temperature in the case of oil/ethanol but decreases for coal tar/water. The capillary number has been found to be low enough (10^{-5}) to justify that capillary forces prevail rather than viscous forces at the pore scale. In addition, no emergence of viscous fingers has been noted during the small pressure step experiments. Thus we can conclude that measurements of capillary pressure – saturation in our case has been done with respect to hypothesis behind generalized Darcy's law, namely the fact that the interface between both liquid phases is rigid and no fingering occurs.

It has been found that viscosity ratio, during imbibition, decreases by a factor 3 for coal tar/water and a factor of 2 for oil/ethanol. Here, the influence of temperature on the viscosity ratio was not as high as expected. Those variations were not sufficient to change the order of magnitude of the dimensionless values and to change the residual saturations. Increasing the temperature has two consequences for the imbibition process: increasing the viscosity ratio and decreasing the capillary number. Also, it appears that the effect of temperature on residual non-wetting phase saturation $S_{r,nw}$ was almost negligible in both cases. However, previous viscous LNAPL and DNAPL displacement experiments have shown that the injection of hot water increases the recovery rate of the contaminant and reduces the residual saturation (Jabbour et al., 1996; O'Carroll and Sleep, 2007). The experiments are done here by increasing the capillary pressure with small pressure steps. Several weeks are needed to complete a drainage and imbibition cycle experiment. The capillary numbers in our quasi-static experiments are still low (Ca << 1), which corresponds to a capillary fingering regime. In this case, the displacement structure is controlled by the fluctuations in the capillary threshold pressures at the displacement front. Thus, the viscosity ratio does not have a visible effect on the results. However, for high invasion rates, the dependence on M may become relevant because of the viscous dominated displacement.

In addition, the dimensionless numbers between coal tar/water and oil/ethanol are quite close. Considering that oil and coal tar are both non-wetting fluids, the same residual saturations and capillary curves between both fluid pairs should be expected. The use of oil/ethanol as a model fluid pair is thereby justified.

4.2. Dynamic effect on two-phase flow properties

As previously noted, two pore-volumes (PV) were needed to reach ethanol irreducible saturation. The injection of oil from the bottom (drainage) into the porous column saturated with ethanol was found to be a stable process at all flow rates. During this step, only ethanol was produced from the cell outlet and as soon as oil reached the cell outlet, only oil was. The displacement front was stable due to gravity effects and because oil's dynamic viscosity is higher than ethanol's (M > 1).

We saw a completely different trend for the injection of 10 PV of ethanol from the top of the cell (imbibition). The following observations were observed for the smallest flow rate (6 mL/min): the injection of 10 PV of ethanol lasted 38 minutes. Only oil was recovered during the first 6 minutes (0 to 1.6 PV). After that, ethanol bubbles started to flow out separately from the system until 10 minutes (1.6 to 2.6 PV). Then, ethanol and oil were both recovered as separate phases at the same time. In the tubing, oil was flowing near the walls while ethanol was recovered near the center (2.6 to 4 PV). Finally, after pumping for 15 minutes (4 to 10 PV), only ethanol was produced for the rest of the injection and the oil saturation did not change.

These saturation changes during oil injection (a) and pumping (b) are shown in Figure 9, for different flow rates and temperature values.

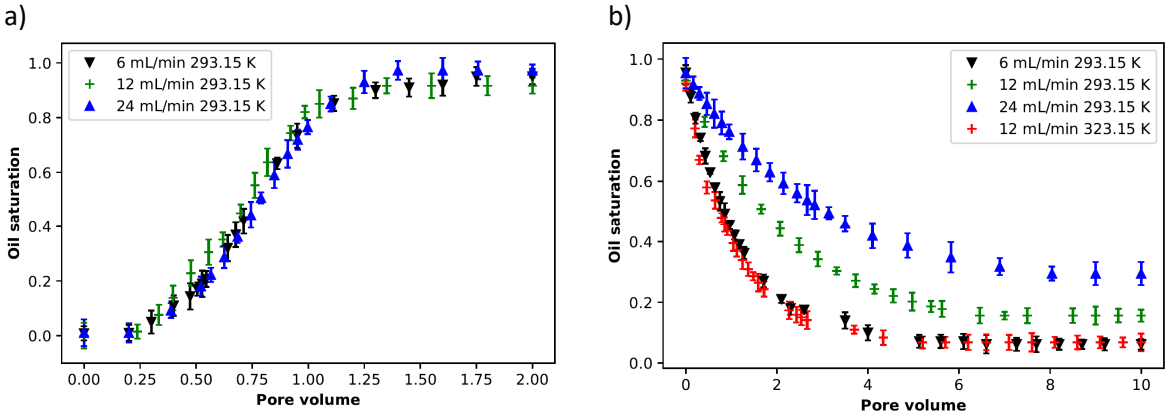

Figure 9: Evolution of ethanol saturation as a function of flow rate during a) the injection (2 PV) and b) pumping (10 PV) of oil

The error bars show the difference between the saturation values calculated from the imaging technique and mass balance. For all saturation points, the maximum saturation difference between both methods is 0.05 (± 1 mL), which validates the proposed imaging technique to determine liquid saturation inside the cell. As shown in Figure 9a, the irreducible saturation $S_{ir,w}$ has been found not to depend on the flow rate. Its value varied between 0.03 (at 6 mL/min) and 0.07 (at 24 mL/min). Also, when the pump was stopped between the injection and pumping steps, there was a small time window where a saturation change occurred. This effect was even more noticeable for a low flow rate. During this time, we noticed saturation redistribution inside the cell likely due to end effects. There are indeed local saturation gradients inside the cell at pore scale that are more important in dynamic conditions. However, we do not take it into account because we mostly focused our study on macroscopic characteristics and measure the mean saturation over the whole cell. Conversely, oil pumping heavily depends on both flow rate and temperature (Figure 9b). First, higher oil residual saturations were obtained for higher flow rates. During the experiments, more ethanol fingers swept a lower area at a high flow rate. This phenomenon had already been observed and confirmed by

(Doorwar and Mohanty, 2015). Consequently, oil saturation decreased at a slower rate even though the pumping rate was higher. Another important point is that residual saturation was obtained with lower pore volumes for low flow rates. Almost 8 PV were needed to reach $S_{r,o}$ = 0.29 at 24 mL/min while only 5 PV were needed with $S_{r,o}$ = 0.06 at 6 mL/min. The comparison between both profiles at 12 mL/min (one obtained at 293.15 K and the other 323.15 K) shows that temperature had two effects. The oil recovery rate was increased at high temperature. During our fluid characterization, we noted that only the viscosity ratio decreased with temperature. Thus, fewer fingers are formed during the injection of ethanol inside oil at 323.15 K, and a higher volume of oil is recovered from the cell. In addition, the residual saturation is smaller at high temperature (0.06 at 323.15 K vs. 0.15 at 293.15 K). However, as we see before, the temperature had no effect on the residual saturation in the quasi-static experiments. Thus, from a certain flow rate (capillary number) where the dynamic effect becomes important, the temperature significantly affects the residual saturation. Finally, the results also underline that with increasing temperature, which leads to a lower viscosity ratio, oil recovery is enhanced at even higher flow rates. This means that the remediation time is shortened at higher temperatures.

The pressure differences between the inlet and outlet of the cell vs. saturation curves during oil injection (a) and pumping (b) are presented in Figure 10, for different flow rates and temperature values.

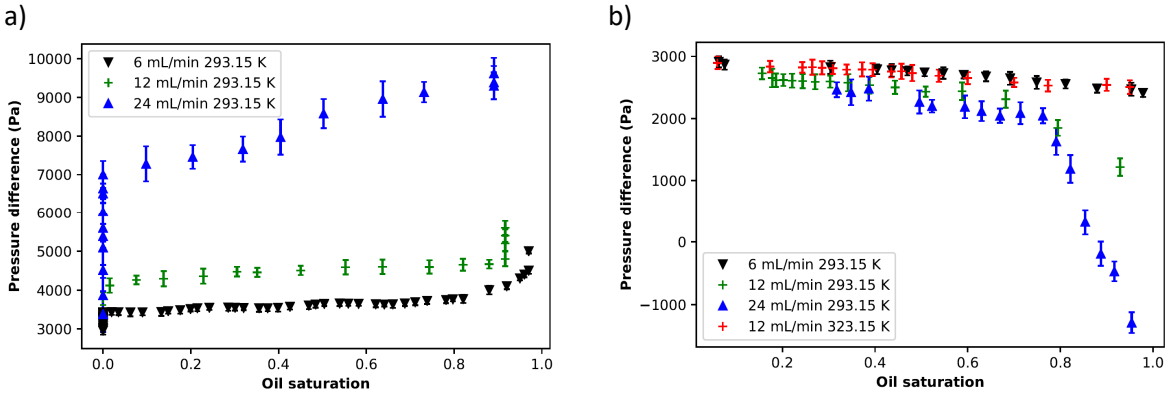

Figure 10: Measured pressure difference during injection (a) and pumping (b) of oil

As mentioned before, we ran the experiments with a volumetric pump. This type of pump keeps a constant flow rate, and pressure adapts itself in consequence. Thus, a higher injection flow rate leads to a higher pressure difference in the system. Conversely, if the pumping flow rate is high, the depression needed will be bigger and can go under atmospheric pressure (defined as a relative pressure equal to 0 Pa here). It is also interesting to note that the pressure required to rotate the pump at 12 mL/min was also lower for higher temperature value (323.15 K).

The cell was at zero oil saturation at the beginning of the oil injection (Figure 8a). The pressure difference inside the cell slowly increased almost linearly until irreducible wetting (ethanol) saturation. The prescribed flow rate at the pump increased the measured pressure difference inside the cell, but no difference in saturation values was observed. At irreducible ethanol saturation, the pressure still increased due to the rise of ethanol level inside the ethanol reservoir situated above the cell.

The cell was at irreducible wetting saturation at the beginning of the oil pumping (Figure 8b). The pressure difference fell almost immediately as soon as pumping began. A higher flow rate translated into a higher initial pressure drop. Then the pressure difference increased linearly until ethanol breakthrough, time at which ethanol starts to be recovered. The pressure difference stabilized at non-wetting (oil) residual saturation.

The pressure needed to pump oil from the cell at 323.15 K was lower than that at 293.15 K. This effect is mainly linked to the reduction of dynamic viscosity. It is possible to interpret this from another point of view: The recovery rate of oil would be higher at 323.15 K than at 293.15 K initially, but the pumping done with the highest flow rate (26 mL/min) is also the pumping that generated the highest residual oil saturation (0.29). A certain balance between operating pressure and temperature needs to be determined for viscous DNAPLs in permeable media to recover the largest volume from the porous media in the smallest time.

A summary of all experiments, dimensionless numbers, irreducible saturations $S_{ir,w,}$ and residual saturations $S_{r,o}$ obtained in this work are presented in Table 3. For dynamic experiments, the characteristic velocity was considered equal to the pump flow rate (in m^3/s) divided by the porous medium section (5.6 cm * 2.5 cm) for capillary number calculations. As seen before for quasi-static experiments, the Bond number can be considered constant. This is because the parameters contributing to capillary forces (interfacial tension, wettability, pore geometry) are invariant with temperature.

Capillary numbers during dynamic experiments were very high ($Ca >> 10^{-2}$) compared to quasi-static ones ($Ca \approx 10^{-5}$). Viscous forces were much more predominant than capillary forces in that case. It should be noted that the reported capillary numbers were obtained in one-dimensional flow conditions. In a real site, the velocity field will change depending on the radial distance from the well. Studies in 2D and 3D experimental setups are needed to better understand the governing conditions that may impact the dynamic effects in real sites. During injection, the flow rates tested gave almost zero irreducible saturation: the oil was able to sweep almost all the ethanol initially inside the cell. The capillary number and mobility ratio were both important to determine the effect of temperature on residual saturation in this case. First, the flow rate increased (Ca increased), leading to a higher residual saturation due to thinner and longer viscous fingers. Then, the dimensionless numbers were almost the same at 6 mL/min at 293.15 K and 12 mL/min at 323.15 K. Thus, it is logical to obtain the same residual saturation. However, it took 10 minutes to reach this value at 323.15 K instead of 40 minutes at 6 mL/min at 293.15 K, validating the use of temperature as a way to enhance DNAPL pumping.

Table 3: Summary of all conducted experiments with their associated Bond number, Capillary number, viscosity ratio, irreducible saturations $S_{ir,w}$, residual saturation S_r, and image observations

Experiment	Temperature (K)	Bo	Ca	M	$S_{ir,w}$ or $S_{r,o}$	Observations
Quasi-static drainage	293.15	4.66×10^{-1}	5.82×10^{-5}	6.19×10^{1}	0.10±0.02	Stable flow with low capillary fingering
Quasi-static drainage	323.15	5.77×10^{-1}	7.21×10^{-5}	3.40×10^{1}	0.11±0.02	Stable flow with low capillary fingering and low film
Injection (6 mL/min)	293.15	4.66×10^{-1}	3.87×10^{0}	6.19×10^{1}	0.05	Stable flow
Injection (12 mL/min)	293.15	4.66×10^{-1}	7.75×10^{0}	6.19×10^{1}	0.07	Stable flow
Injection (24 mL/min)	293.15	4.66×10^{-1}	1.50×10^{1}	6.19×10^{1}	0.03	Stable flow
Quasi-static imbibition	293.15	4.66×10^{-1}	5.82×10^{-5}	1.64×10^{-2}	0.14±0.02	Transition between capillary and viscous fingering
Pumping (6 mL/min)	293.15	4.66×10^{-1}	6.50×10^{-2}	1.64×10^{-2}	0.06	High films and low viscous fingering
Pumping (12 mL/min)	293.15	4.66×10^{-1}	1.30×10^{-1}	1.64×10^{-2}	0.16	Moderate films and viscous fingering
Pumping (24 mL/min)	293.15	4.66×10^{-1}	2.60×10^{-1}	1.64×10^{-2}	0.29	Low films and high viscous fingering
Pumping (12 mL/min)	323.15	5.77×10^{-1}	4.80×10^{-2}	2.91×10^{-2}	0.06	High films, low viscous fingering
Quasi-static imbibition	323.15	5.77×10^{-1}	7.21×10^{-5}	2.91×10^{-2}	0.13±0.03	Transition between capillary and viscous fingering

The generalized Darcy's law with the use of relative permeability is often used in order to understand the effect of temperature. However, in the case of injection or pumping in highly permeable media, dynamic effects must be considered and cannot be represented by this law accurately. The theoretical notion of relative permeability is compromised due to the presence of viscous fingering and ethanol films around the glass beads. In this situation, it is difficult to admit the hypothesis that both phases are flowing separately in the medium. The fact that temperature reduces oil residual saturation appears to be linked to this.

Also, we noted the presence of ethanol films in all experiments under dynamic conditions. These films are generally not taken into account in numerical studies considering the effect of temperature. Their emergence was even higher when the temperature had been increased. No experimental study has been conducted on fluid film behavior, and it is, therefore, difficult to highlight if this is an experimental artifact due to the fluids used or a phenomenon that should be taken into account. Yet, when approaching residual saturation values, the number of films decreases and becomes even less visible as the capillary number becomes high. The presence of these films has been observed in the past in trickle-bed reactors (Reinecke and Mewes, 1997). The solid particle size used in this type of reactors is in the millimeter range, like the ones studied here. This leads us to conclude that the presence and retention of these films inside a porous medium are mostly linked to the high capillary

number encountered in highly permeable porous media. Moura *et al.* (2019) have also observed the presence of capillary bridges during drainage experiments. Their results show that film flow can enhance the recovery of the trapped liquid (Moura et al., 2019). This is coherent with our observations: more films are present during imbibition at 323.15 K than at 293.15 K and the resulting ethanol saturation is then reduced.

Pressure difference and ethanol saturation data have been used in order to determine relative permeability curves with the JBN method (Welge, 1952; Johnson et al., 1959). Qin et al. (2018) previously measured oil and water relative permeabilities in sand packs and determined that temperature effectively increases both fluids relative permeabilities (Qin et al., 2018). Figure 11 represents the effect of temperature on oil and ethanol relative permeability measured in pumping conditions at 12 mL/min.

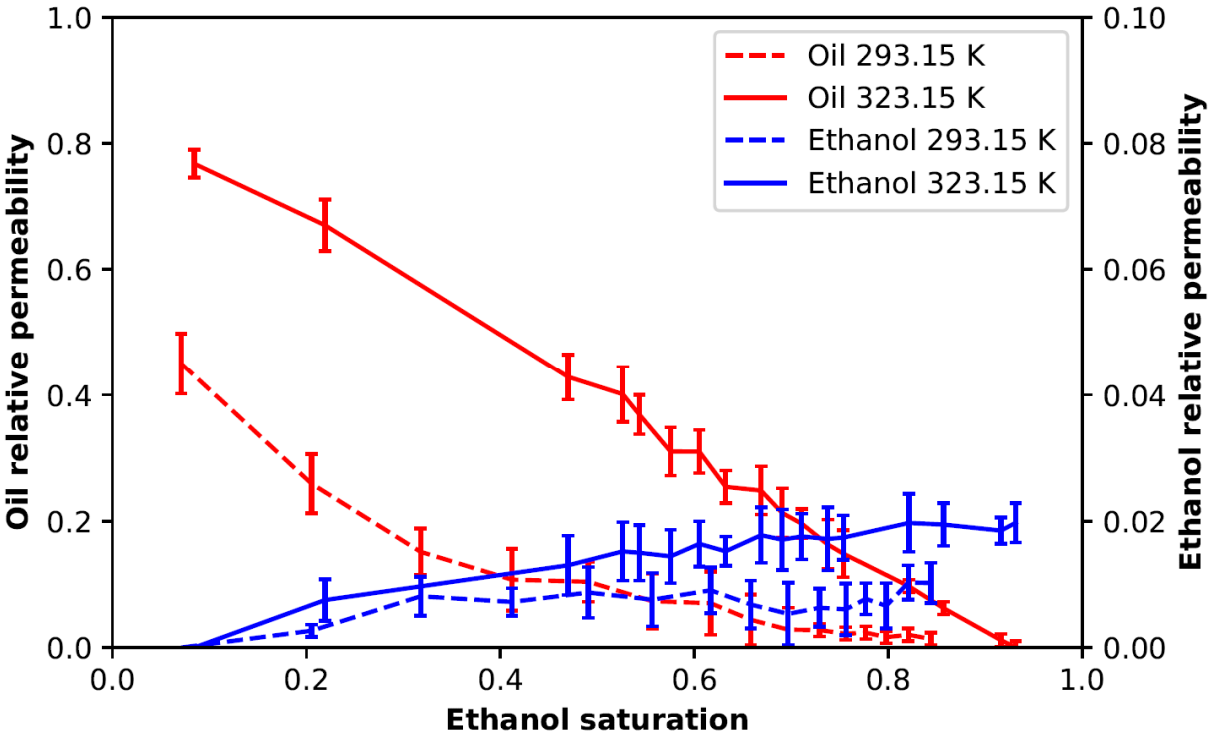

Figure 11: Oil and ethanol relative permeabilities estimated during pumping at 12 mL/min at 293.15 K and 323.15 K

Oil relative permeabilities have been found to have an exponential profile at 293.15 K and an almost linear profile at 323.15 K. Ethanol relative permeabilities have a small magnitude compared to oil relative permeability, due to the high viscosity ratio considered in our study. In addition, ethanol relative permeability increases with temperature. For all saturations, oil and ethanol relative permeabilities are higher at 323.15 K rather than at 293.15 K. This is due to the difference in saturation profiles between pumping at 293.15 K and 323.15 K. Both oil and ethanol are thus able to flow at a faster rate in pumping applications for higher temperature.

5. Conclusions

Changing soil temperature during DNAPL pure phase recovery involves analyses of the parameters used in generalized Darcy's law. Hypotheses behind the use of this equation were recalled and it appears that in soil remediation applications, wetting phase film and viscous fingering may appear under dynamic conditions. The influence of temperature on a coal tar sampled from a field was investigated. Density, dynamic viscosity, interfacial tension, and contact angle parameters for coal tar/water and oil/ethanol (a model two-phase liquid) have been measured between 293.15 K and 323.15 K. Dynamic viscosities of all studied liquids decrease exponentially with temperature. Liquids densities and interfacial tensions between the two immiscible coupled fluids decrease linearly with temperature. These parameters are all important in the capillary and viscous forces balance determining the flow regime. The studies on the expected flow pattern have been investigated by (Lenormand et al., 1988). The further analysis of dimensionless numbers between both fluid pairs showed that it is possible to use oil and ethanol as a model fluid for studying coal tar-water two-phase flow in porous media.

We performed drainage and imbibition experiments in a 1D porous cell under almost quasi-static ($Ca < 10^{-5}$) conditions and in the application range of generalized Darcy's law. During the experiments, no viscous fingering was noted. Nor was a temperature effect observed on two-phase flow van Genuchten parameters or residual saturations for both couples of liquids at 293.15 K and 323.15 K. It should be noted that capillary forces are relatively small in these cases. This is because of the highly permeable porous medium used and the low interfacial tension of the considered liquids.

In all our drainage/imbibition experiments, the residual saturations and observations obtained with canola oil and ethanol experiments were close to the ones observed with coal tar and water. However, it is considerably easier to obtain results with simple and almost not toxic liquids, like canola oil and ethanol, especially by image analyzing techniques. This type of simplification is done with glass beads in experiments to model a simpler and inert porous medium with the same permeability and porosity.

Finally, we further studied the effect of temperature by pumping oil in the small cell filled by the glass beads at irreducible ethanol saturation and 323.15 K. Increasing the temperature reduces the pressure difference needed to reach the same pumping rate, increases the recovery rate of oil from the porous medium ($S_{r,o}$ = 16% down to 6% when heating from 293.15 K to 323.15 K), and finally increases both oil and ethanol relative permeabilities. The higher recovery rate is linked not only to reduced viscous fingering but also to the presence of interfacial films that seem to appear because of the high capillary numbers ($Ca > 10^{-2}$) encountered in highly permeable media. Residual saturation has also been found to decrease considerably due to decreasing the viscous fingering occurred at low flow rate. The presence and growth of viscous fingerings allow the ethanol to flush a larger part of the medium. The experiments performed under dynamic conditions have shown that dynamic effects are important when considering temperature effects during pumping operations. In complement to our study which focuses on macroscopic quantities, it would be interesting to extract local and microscopic quantities to investigate more thoroughly the impact of temperature on two-phase flow in a real site. The coupling between heat transfers and two-phase flow should be also considered in order to better understand the physical mechanisms happening during thermally enhanced DNAPL pumping.

6. Acknowledgments

This study was performed as part of the “Bioxyval” project. The authors would like to thank ADEME for co-funding the project under the “AMI” program, REMEA, and ANRT for providing the PhD grant for Nicolas Philippe. We gratefully acknowledge the financial support provided to the PIVOTS project by the “Région Centre – Val de Loire” and the European Regional Development Fund.

7. References

Andrade, E.N.C., 1940. The viscosity of liquids. Proceedings of the Physical Society 52, 748.

Bachmann, J., Horton, R., Grant, S.A., Ploeg, R.R. van der, 2002. Temperature Dependence of Water Retention Curves for Wettable and Water-Repellent Soils 66, 44.

Baker, R.S., LaChance, J., Heron, G., 2006. In-pile thermal desorption of PAHs, PCBs and dioxins/furans in soil and sediment. Land Contamination & Reclamation 14, 620–624.

Baston, D.P., Falta, R.W., Kueper, B.H., 2010. Numerical Modeling of Thermal Conductive Heating in Fractured Bedrock. Ground Water 48, 836–843.

Berry, J.D., Neeson, M.J., Dagastine, R.R., Chan, D.Y.C., Tabor, R.F., 2015. Measurement of surface and interfacial tension using pendant drop tensiometry 454, 226–237.

Bhatia, G., Aggarwal, R.K., Chari, S.S., Jain, G.C., 1977. Rheological characteristics of coal tar and petroleum pitches with and without additives. Carbon 15, 219–223.

Brown, D.G., Gupta, L., Kim, T.-H., Keith Moo-Young, H., Coleman, A.J., 2006. Comparative assessment of coal tars obtained from 10 former manufactured gas plant sites in the Eastern United States. Chemosphere 65, 1562–1569.

Cai, Z.T., Mohanty, K.K., 1997. Interfacial Tension Measurement in DNAPL/Aqueous Surfactant Systems. Journal of Colloid and Interface Science 195, 408–410.

Chatzis, I., Morrow, N.R., 1984. Correlation of capillary number relationships for sandstone. Society of Petroleum Engineers Journal 24, 555–562.

Colombano, S., Davarzani, H., Hullebusch, E.D. van, Huguenot, D., Guyonnet, D., Deparis, J., Ignatiadis, I., 2020. Thermal and chemical enhanced recovery of heavy chlorinated organic compounds in saturated porous media: 1D cell drainage-imbibition experiments. Science of The Total Environment 706, 135758.

Cueto-Felgueroso, L., Juanes, R., 2009. A phase field model of unsaturated flow. Water resources research 45.

Darnault, C.J.G., Throop, J.A., DiCarlo, D.A., Rimmer, A., Steenhuis, T.S., Parlange, J.-Y., 1998. Visualization by light transmission of oil and water contents in transient two-phase flow fields. Journal of Contaminant Hydrology 31, 337–348.

Davis, E.L., 1994. Effect of temperature and pore size on the hydraulic properties and flow of a hydrocarbon oil in the subsurface. Journal of Contaminant Hydrology 16, 55–86.

Davis, E.L., 1997. How heat can enhance in-situ soil and aquifer remediation: important chemical properties and guidance on choosing an appropriate technique. U.S. Environmental Protection Agency, Groundwater Issue Paper, EPA/540/S-97/502.

Davit, Y., Quintard, M., 2019. One-Phase and Two-Phase Flow in Highly Permeable Porous Media. Heat Transfer Engineering 40, 391–409.

Dawson, H.E., Roberts, P.V., 1997. Influence of Viscous, Gravitational, and Capillary Forces on DNAPL Saturation. Groundwater 35, 261–269.
Ding, D., Song, X., Wei, C., LaChance, J., 2019. A review on the sustainability of thermal treatment for contaminated soils. Environmental Pollution 253, 449–463.
Donahue, D.J., Bartell, F.E., 1952. The boundary tension at water-organic liquid interfaces. The Journal of Physical Chemistry 56, 480–484.
Doorwar, S., Mohanty, K.K., 2015. Fingering function for unstable immiscible flows, in: SPEReservoirSimulationSymposium. Society of Petroleum Engineers.
Dury, O., Fischer, U., Schulin, R., 1998. Dependence of hydraulic and pneumatic characteristics of soils on a dissolved organic compound. Journal of contaminant hydrology 33, 39–57.
Emanuel, A.S., Cook, G.W., 1974. Pseudo-Relative Permeability for Well Modeling. Society of Petroleum Engineers Journal 14, 7–9.
Esmaeili, S., Sarma, H., Harding, T., Maini, B., 2019. Review of the effect of temperature on oil-water relative permeability in porous rocks of oil reservoirs. Fuel 237, 91–116.
Fitzer, E., Kompalik, D., Yudatet, K., 1987. Rheological characteristics of coal-tar pitches. Fuel 66, 1504–1511.
Fulton, T.E. D.E. Reuter G.J. Buscheck, 1991. Hot water enhanced recovery of phase separated lubricating oil. Proceedings of the Petroleum Hydrocarbons and Organic Chemicals in Ground Water: Prevention, Detection, and Restoration Conference and Exposition, pp. 143-156.
Gaonkar, A.G., 1989. Interfacial tensions of vegetable oil/water systems: effect of oil purification. Journal of the American Oil Chemists' Society 66, 1090–1092.
Geel, P.J.V., Sykes, J.F., 1994. Laboratory and model simulations of a LNAPL spill in a variably-saturated sand, 1. Laboratory experiment and image analysis techniques. Journal of Contaminant Hydrology 17, 1–25.
Gerhard, J.I., Kueper, B.H., 2003. Relative permeability characteristics necessary for simulating DNAPL infiltration, redistribution, and immobilization in saturated porous media. Water Resour. Res. 39.
Hagoort, J., 1974. Displacement stability of water drives in water-wet connate-water-bearing reservoirs. Society of Petroleum Engineers Journal 14, 63–74.
Hasan, T., Gerhard, J.I., Hadden, R., Rein, G., 2015. Self-sustaining smouldering combustion of coal tar for the remediation of contaminated sand: Two-dimensional experiments and computational simulations. Fuel 150, 288–297.
Hassanizadeh, S.M., Gray, W.G., 1993. Thermodynamic basis of capillary pressure in porous media. Water resources research 29, 3389–3405.
Hearn, C.L., 1971. Simulation of Stratified Waterflooding by Pseudo Relative Permeability Curves. Journal of Petroleum Technology 23, 805–813.
Iravani, M.A., Deparis, J., Davarzani, H., Colombano, S., Guérin, R., Maineult, A., 2020. The influence of temperature on the dielectric permittivity and complex electrical resistivity of porous media saturated with DNAPLs: A laboratory study. Journal of Applied Geophysics 172, 103921.
Jabbour, C., Quintard, M., Bertin, H., Robin, M., 1996. Oil recovery by steam injection: three-phase flow effects. Journal of Petroleum Science and Engineering 16, 109–130.
Johansson, C., Bataillard, P., Biache, C., Lorgeoux, C., Colombano, S., Joubert, A., Pigot, T., Faure, P., 2019. FerrateVI oxidation of polycyclic aromatic compounds (PAHs and polar PACs) on DNAPL-spiked sand: degradation efficiency and oxygenated by-product formation compared to conventional oxidants. Environmental Science and Pollution Research.
Johnson, E.F., Bossler, D.P., Bossler, V.O., 1959. Calculation of relative permeability from displacement experiments.
Kalaydjian, F.J.-M., 1992. Dynamic Capillary Pressure Curve for Water/Oil Displacement in Porous Media: Theory vs. Experiment. SPE Annual Technical Conference and Exhibition.
Kavanaugh, M., Kresic, N., 2008. Groundwater Management in Large River Basins, in: M. Dimkic, H.J.B., Kavanaugh, M. (Eds.), IWA Publishing, pp. 520–600.

Koci, X., Quintard, M., Robin, M., Gadelle, C., 1989. Effet de la température sur les propriétés de déplacement polyphasique en milieux poreux. Revue de l'Institut français du pétrole 44, 763–783.

Kong, L., 2004. Characterization of Mineral Oil, Coal Tar and Soil Properties and Investigation of Mechanisms that Affect Coal Tar Entrapment In and Removal From Porous Media. Ph.D. dissertation, School of Civil and Environmental Engineering. Georgia Institute of Technology, Atlanta, 309 pp.

Lenormand, R., Touboul, E., Zarcone, C., 1988. Numerical models and experiments on immiscible displacements in porous media. Journal of fluid mechanics 189, 165–187.

McDade, J.M., McGuire, T.M., Newell, C.J., 2005. Analysis of DNAPL source-depletion costs at 36 field sites. Remediation 15, 9–18.

McLaren, S., Worboys M., Speake O., P., M., 2009. Ex-situ Thermally Enhanced Coal Tar Recovery - A Low Carbon Option.

Melin, E., Jarvinen, K., Puhakka, J., 1998. Effects of temperature on chlorophenol biodegradation kinetics in fluidized-bed reactors with different biomass carriers. Water Research 32, 81–90.

Moura, M., Flekkøy, E.G., Måløy, K.J., Schäfer, G., Toussaint, R., 2019. Connectivity enhancement due to film flow in porous media. Physical Review Fluids 4, 094102.

Muskat, M., Meres, M.W., 1936. The flow of heterogeneous fluids through porous media. Physics 7, 346–363.

Navy, 2008. Plume management zone to manage chlorinated solvents. Naval Weapons Industrial Reserve Plant, Dallas, Texas, USA. Department of the Navy Environmental Restoration Program 2008 progress report, p. 32.

Newell, C.J., Farhat, S.K., Adamson, D.T., Looney, B.B., 2011. Contaminant Plume Classification System Based on Mass Discharge. Ground Water 49, 914–919.

O'Carroll, D.M., Phelan, T.J., Abriola, L.M., 2005. Exploring dynamic effects in capillary pressure in multistep outflow experiments. Water Resources Research 41.

O'Carroll, D.M., Sleep, B.E., 2007. Hot water flushing for immiscible displacement of a viscous NAPL 91, 247–266.

Pape, A., Switzer, C., McCosh, N., Knapp, C.W., 2015. Impacts of thermal and smouldering remediation on plant growth and soil ecology. Geoderma 243-244, 1–9.

Qin, Y., Wu, Y., Liu, P., Zhao, F., Yuan, Z., 2018. Experimental studies on effects of temperature on oil and water relative permeability in heavy-oil reservoirs. Scientific reports 8, 12530.

Rein, G., 2009. Smouldering Combustion Phenomena in Science and Technology.

Reinecke, N., Mewes, D., 1997. Investigation of the two-phase flow in trickle-bed reactors using capacitance tomography. Chemical Engineering Science 52, 2111–2127.

Russell, K.T., Rabideau, A.J., 2000. Decision Analysis for Pump-and-Treat Design. Ground Water Monitoring & Remediation 20, 159–168.

Sanaiotti, G., Silva, C.A.S. da, Parreira, A.G., Tótola, M.R., Meirelles, A.J.A., Batista, E.A.C., 2010. Densities, Viscosities, Interfacial Tensions, and Liquid−Liquid Equilibrium Data for Systems Composed of Soybean Oil + Commercial Linoleic Acid + Ethanol + Water at 298.2 K. J. Chem. Eng. Data 55, 5237–5245.

Scholes, G.C., Gerhard, J.I., Grant, G.P., Major, D.W., Vidumsky, J.E., Switzer, C., Torero, J.L., 2015. Smoldering Remediation of Coal-Tar-Contaminated Soil: Pilot Field Tests of STAR. Environmental Science & Technology 49, 14334–14342.

Schwille, F., Pankow, J.F., 1988. Dense chlorinated solvents in porous and fractured media - Model experiments. Lewis Publishers,Chelsea, MI, United States.

Sleep, B.E., Ma, Y., 1997. Thermal variation of organic fluid properties and impact on thermal remediation feasibility. Journal of Soil Contamination 6, 281–306.

Smith, J.E., Zhang, Z.F., 2001. Determining effective interfacial tension and predicting finger spacing for DNAPL penetration into water-saturated porous media. Journal of Contaminant Hydrology 48, 167–183.

Switzer, C., Pironi, P., Gerhard, J.I., Rein, G., Torero, J.L., 2009. Self-Sustaining Smoldering Combustion: A Novel Remediation Process for Non-Aqueous-Phase Liquids in Porous Media 43, 5871–5877.

USEPA, 1996. Pump and Treat Ground Water Remediation A Guide for Decision Makers and Practitioners. EPA/625/R-95/005.

Vargaftik, L.D. N. B. Volkov B. N. & Voljak, 1983. International tables of the surface tension of water. Journal of Physical and Chemical Reference Data 817–820.

Wang, J., Dong, M., Asghari, K., 2006. Effect of oil viscosity on heavy oil-water relative permeability curves, in: SPE/DOESymposium Improved Oil Recovery. Society of Petroleum Engineers.

Watson, F., Maes, J., Geiger, S., Mackay, E., Singleton, M., McGravie, T., Anouilh, T., Jobe, T.D., Zhang, S., Agar, S., Ishutov, S., Hasiuk, F., 2019. Comparison of Flow and Transport Experiments on 3D Printed Micromodels with Direct Numerical Simulations. Transport in Porous Media 129, 449–466.

Welge, H.J., 1952. A simplified method for computing oil recovery by gas or water drive. Journal of Petroleum Technology 4, 91–98.

Whitaker, S., 1986. Flow in porous media II: The governing equations for immiscible, two-phase flow. Transport in Porous Media 1, 105–125.

Wu, M., Cheng, Z., Wu, J., Wu, J., 2017. Estimation of representative elementary volume for DNAPL saturation and DNAPL-water interfacial areas in 2D heterogeneous porous media. Journal of Hydrology 549, 12–26.

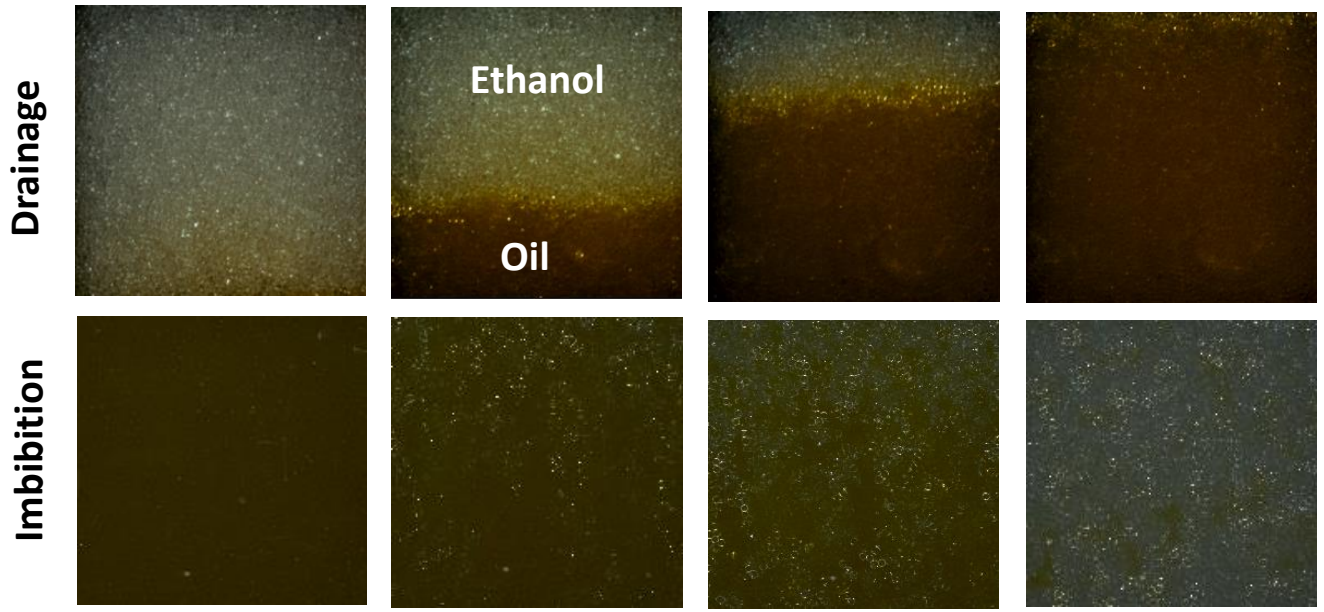

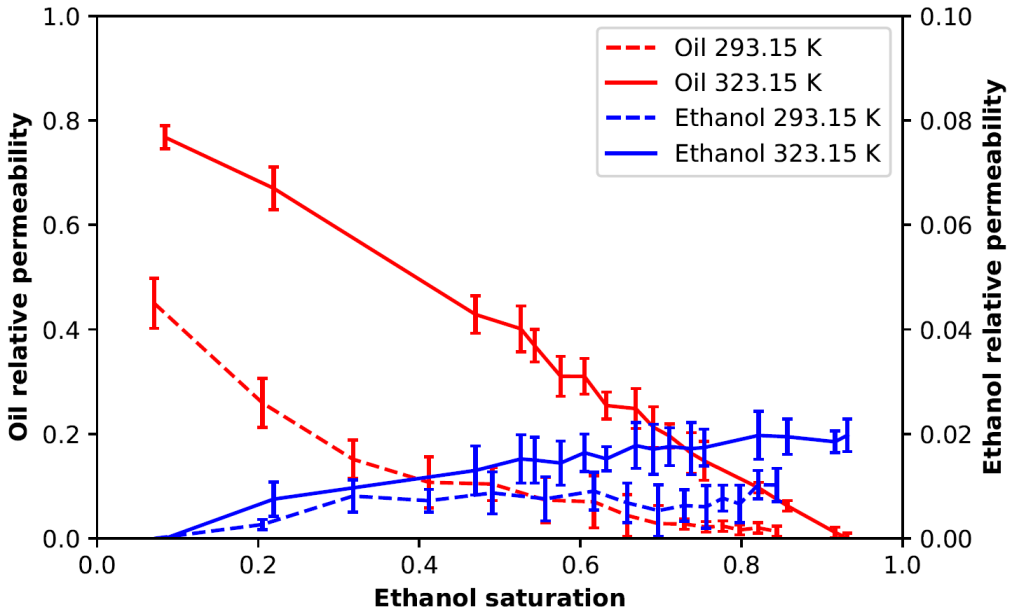

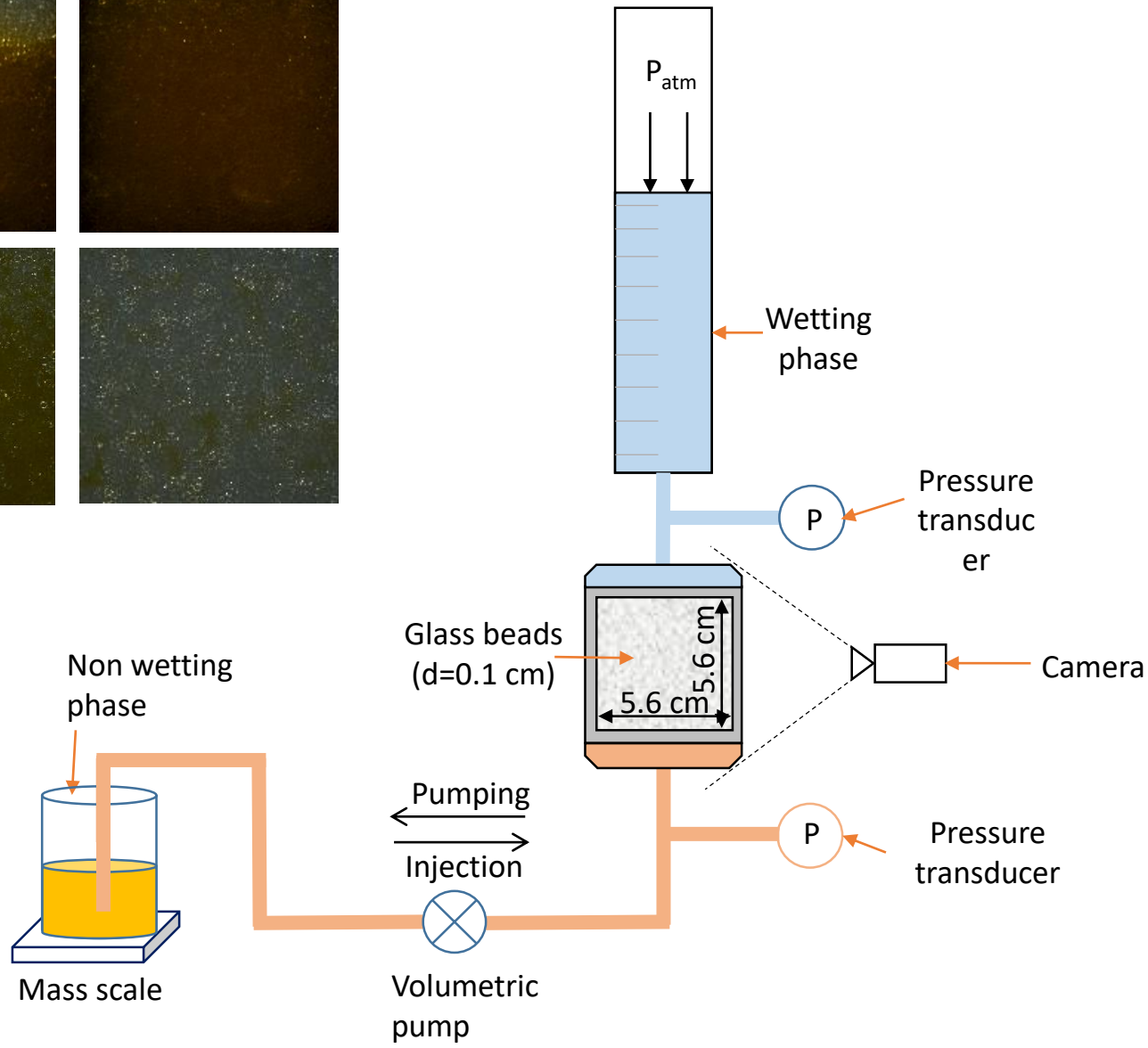

Dynamic drainage-imbibition experimental setup (2D cell)